IMPROVED MODELLING OF HARMATTAN DUST EFFECT ON THE CROSS POLARIZATION OF A MICROWAVE ACCESS RADIO LINK OPERATING BETWEEN 15GHz AND 38GHz

BY

HENRY AIKHIONBARE

Department of Electrical & Computer Engineering,

Faculty of Engineering,

Ahmadu Bello University,

Zaria

March, 2017

IMPROVED MODELLING OF HARMATTAN DUST EFFECT ON THE CROSS POLARIZATION OF A MICROWAVE ACCESS RADIO LINK OPERATING BETWEEN 15GHz AND 38GHz

BY

Henry AIKHIONBARE

B.Eng.(ABU), 2008

(P13EGCM8030)

efosahenry@yahoo.com

A DISSERTATION SUBMITTED TO THE DEPARTMENT OF ELECTRICAL AND COMPUTER ENGINEERING, AHMADU BELLO UNIVERSITY, ZARIA IN PARTIAL FULFILLMENT OF THE REQUIREMENTS FOR THE AWARD OF MASTER OF SCIENCE (M.Sc.) DEGREE IN TELECOMMUNICATIONS ENGINEERING

March, 2017

DECLARATION

I, Henry AIKHIONBARE, declare that this dissertation titled “Improved Modelling of Harmattan Dust Effect on the Cross Polarization of a Microwave Access Radio Link Operating Between 15GHz and 38GHz” was carried out by me in the Department of Electrical and Computer Engineering. The information derived from literature has been duly acknowledged in the text and a list of references provided. To the best of my knowledge, no part of this dissertation was previously presented for another degree or diploma at this or any other institution.

Henry AIKHIONBARE

Signature Date

CERTIFICATION

This dissertation titled "IMPROVED MODELLING OF HARMATTAN DUST EFFECT ON THE CROSS POLARIZATION OF A MICROWAVE ACCESS RADIO LINK OPERATING BETWEEN 15GHz AND 38GHz" by Henry AIKHIOBARE meets the requirements for the award of degree of Master of Science (MSc) in Telecommunications Engineering by Ahmadu Bello University, Zaria and it is approved for its contribution to knowledge and literary presentation.

Dr. S.M. Sani
(Chairman, Supervisory Committee) Signature Date

Dr. A.M.S Tekanyi
(Member, Supervisory Committee) Signature Date

Dr. Y. Jibril
(Head of Department) Signature Date

Prof. S.Z. Abubakar
(Dean, School of Postgraduate Studies) Signature Date

DEDICATION

This research project is dedicated to God Almighty who gave me the grace and determination to complete the program within specified time.

ACKNOWLEDGEMENTS

All praise and thanks is due to God almighty for His love, mercy, faithfulness, divine provision and protection throughout my life and the period of this research work.

My sincere thanks go to my lovely wife Josephine who sacrificed so many things for the whole period of this study. I pray that the Almighty God bless you.

I would like to appreciate the moral and spiritual support of my parents Professor Henry Aikhionbare and Mrs Vivian Aikhionbare, my siblings Joy Babaoye, Henrietta Etukudo and Rebecca Ojiri. Words cannot express my deepest gratitude.

I would like to sincerely express my profound gratitude to my supervisors, Dr. S.M. Sani and Dr. A.M.S Tekanyi for their valuable contributions and support throughout this research work. I am grateful to Dr. S.M. Sani for providing fundamental insights and guidance. I really appreciate his constant moral advice, follow-up and encouragement. I appreciate him for the confidence he built in me over this period. I sincerely believe the completion of this work is due to him. He is my mentor for life. I really appreciate Dr A.M.S Tekanyi for his understanding and timely intervention. The fact that he always had time for me and the valuable insights he brought to this work and valuable lessons he taught me about life.

My appreciation also goes to the Head of Department Dr. Y.Jibril for initiating policies and actions to motivate all students. I would also like to appreciate Prof. M. B. Mu'azu, for his constructive criticism and valuable contributions.

I would also like to acknowledge the contributions of my mentor and friend in person of Engr. Mohammed Abdullahi. He has been very instrumental in proof reading and correcting this work. I thank Mr Elvis Obi, Mr Bashir Sadiq Olaniyi, and Mr Abdulrahman Olaniyan for their valuable contributions and taking time out of their busy schedule to go through my manuscript. I am highly indebted to all my lecturers who taught me: Prof. B. G. Bajoga, Dr. D. D. Dajab, Dr. S. Garba, Dr. A.D Usman, Engr. Zanna, Dr Olaitan Akinsanmi and all those whose names could not be mentioned. My appreciation also goes to Mallam Abdullahi Tukur for his administrative support.

I wish to acknowledge Etisalat, Nigeria for initiating and sponsoring the Etisalat Telecommunications Engineering Program (ETEP). The series of trainings and internship have really broadened my knowledge and experience.

I wish to acknowledge my Company of employment Aviat Networks for work flexibility to enable program completion.

I appreciate my office superiors, Adekunle Adebisi, Sayo Olawole, Adekunbi Agboola and Olawale Osimosu.

I appreciate my friends and colleagues: Maxwell Aniakor, Damian, Ayuba Danburam, Ismail Mohammed, Benjamin Dzer, Mohammed Saliu Momodu, Abdulsalam Mustapha, Saint Labi, Patrick Ajeye, Nathan Bello, Ahmed Adanma, Jeremiah Ejike, Samuel Ailen-Ubhi, Adeyemi Adepoju, Ayo Adeniran, Alaba Adeyemi and all other friends who have affected my life in one way or the other.

And finally I appreciate my Boss Babatunde Hussain who is one that has unknowingly shaped my life in more ways than one.

TABLE OF CONTENTS

LIST OF FIGURES

LIST OF TABLES

LIST OF ABBREVIATIONS

BSC	Base Station Controller
BTS	Base Transceiver System
dB	decibel
dBm	decibel relative to one milliwatt
GHz	Giga Hertz
GSM	Global System for Mobile Communications
HF	High Frequency
kg	kilogram
km	kilometer
LOS	Line of Sight
m	meter
MSC	Mobile Switching Center
NIMET	Nigerian Meteorological Agency
PSTN	Private Switched Telephone Network
RF	Radio Frequency
Rx	Receiver
Tx	Transmitter
XPD	Cross Polarization Discrimination

ABSTRACT

Dust carry non-spherical particles which in the absence of turbulence or shear wind and hydrodynamic forces, tend to orient their major axis in the vertical plane, thus resulting in particles anisotropy which may contribute to Cross Polarization Discrimination (XPD) degradation due to differential phase shift. This research presents an improved model of harmattan dust effect on cross polarization of microwave access radio link operating between 15GHz and 38GHz. Meteorological data such as dust mass concentration, visibility, etc. for ten years (that is, 2003 to 2012) were obtained from Nigerian Meteorological Agency (NIMET) and the five months harmattan period data was sorted out. The sorted data were used to deduce important parameters like dielectric constant, relative particle volume and so on. Then, the complex propagation coefficients (attenuation and phase shift) were deduced as a function of wave frequency, media dielectric constant depolarization factor and fractional volume of dust storm using Maxwell's electromagnetic equation for a random medium. Mathematical background for XPD was then established as a function of signal frequency, dielectric constant of dust storm, particle size probability distribution function and visibility. Finally, a link budget analysis was done for some selected frequency values of 18 GHz, 23 GHz, 27 GHz, 30 GHz and 35 GHZ to deduce a fade margin of 52.073dB, 50.5313dB, 41.2168dB, 43.1843dB, 41.6434dB and 41.3091dBrespectively due to the depolarization factor of harmattan period in Kano. A percentage time availability of 99.99 percent was obtained for the selected antenna thereby showing the validity of the developed model based on Rayleigh's distribution Model for Link availability.

CHAPTER ONE

INTRODUCTION

1.1 Background of Study

Wireless communications service providers are currently facing challenges due to the congested radio spectrum which has imposed the use of higher frequencies. However, higher frequency bands are more sensitive to weather conditions and microwave signal degradation due to rapid increase in atmospheric particles.(Elsheikh *et al.*, 2010).

The termgeographical dust usually refers to solid inorganic particles that are derived from the weathering of rocks. In the geological sciences, dust is defined as particles with diameters smaller than 62.5 μm. In the atmospheric sciences, dust is usually defined as the material that can be readily suspended by wind (Shao, 2008).

Increase in frequency of occurrence of dust storm has made the study of wind-blown dust particles as well as their effects on human activities an important topic for research. Appreciable interest has been expressed in the problem associated with influence of dust storm on microwave link performance(Kok *et al.*, 2012). This has been largely attributed to the continuous growth of satellite and terrestrial microwave systems and the use of higher frequencies. There is now spectral congestion of microwave radio frequency range owing to the emergence of new technologies and high demand of telecommunication applications, such as mobile video traffic and other multimedia applications over the past decade. This has given rise to a steady move towards higher carrier frequencies for increased information transfer rates and to further miniaturize equipment for portability. However, a range of meteorological phenomena such as dust storm make microwave propagation a serious problem as operations can be hampered by attenuation due to dust storm particles (Musa *et al.*, 2014a)

1.2 Significance of Research

The research is important to discover the effect of dust on microwave access links operating in regions prone to harmattan dust. The results can then be used to deduce the depolarization loss and then effectively calculate link budgets in these regions to reduce link outages during the harmattan season.

1.3 Statement of Problem

The reliability of microwave signals operating in areas that have high rainfall, a lot of obstacles,where dust and other particles are abundant in air is limited. The effect of dust on microwave signals have attracted interest of researchers because dust is associated with poor visibility which causes high attenuation in the long run. Therefore, there is a need to consider the effect of dust (for areas having abundant dust quantity in air)when developing models for cross polarization of microwave access radio links and when designing a link budget to ensure precision in the fade margin calculation. Thus, the motivation was to investigate the phenomenon of depolarization of microwave signal, propagating through atmosphere having dust particles. The factors of dust size parameter, frequency of incident wave, the angle of incident, and dust permittivity, dust storm visibility and water content analysis was taken into consideration to obtain cross-pole discrimination of electromagnetic wave propagation in the dust storm. Finally, a loss margin due to depolarization was computed from XPD results. This loss margin was added to the traditional link margin calculation for microwave line of sight path planning within the telecommunication radio access frequency range of 15 to 38 GHz.

1.4 Aim and Objectives

The aim of this research work was to examine the effect of dust storm on the cross polarization of a microwave access radio link operating between 15GHz to 38GHz in order to establish an improved mathematical model which includes loss margin due to XPD

degradation for fade margin calculation. This loss margin was added to the traditional fade margin calculation for microwave line of sight link at the microwave radio access network.

The objectives of this research were as follows:

i. Establish a mathematical relationship between XPD and the variables (particle size density, visibility, propagation frequency and permittivity).
ii. Establish a loss margin due to XPD degradation using deduced XPD values and a line of sight fade margin due to XPD degradation.
iii. Design link budget template to account for losses due to dust depolarization.

1.5 Methodology

The following steps were taken to achieve the objectives:

i. Solving Maxwell's electromagnetic equation in the random medium (dust storm medium) to deduce complex propagation coefficients (attenuation and phase constant) as functions of variables including wave frequency, media dielectric constant, depolarization factor and fractional volume of dust particles.
ii. Deduction ofthe mathematical relationship between visibility and fractional volume of dust particle.
iii. Using meteorological data in Kano to deduce dielectric constant.
iv. Establishing:
    a. Probability distribution function from particle size distribution data.
    b. Mathematical relationship between XPD as a function of signal frequency, dielectric constant of dust storm, particle size probability distribution function, and visibility at foremost.
v. Deduction of the fade Margin due to wave depolarization of a co-channel dual polarized microwave transmission link
vi. Modelling and programming using MATLAB R2015b and validation of results.

1.5 Dissertation Organization

The organization of this dissertation report is as follows: Chapter one presents the general background of the study. In Chapter two, review of fundamental concepts pertinent to this research work and detailed review of similar works were presented. Chapter three covers detailed explanation of methods and materials used in this work and Chapter fourcentres onthe results and discussions. In Chapter five, conclusions, significant contributions, limitations and recommendations are presented.The references quoted in this dissertation report as well as appendices have also been provided.

CHAPTER TWO

LITERATURE REVIEW

2.1 Introduction

This Chapter presents a review of the fundamental concepts such as microwave systems and applications, radio waves transmission and losses and so on. It also presents a critical review of previously published research works which are considered very similar to this research.

2.2 Review of Fundamental Concepts

Some fundamentals such as microwave propagation basics, radio waves characteristics, dust storm characteristics amongst others are presented in this chapter. Included also are concepts and model equations relevant to this research.

2.3 Microwave Propagation Fundamentals

Electromagnetic waves which have frequencies that are greater than that of the television signals are known as microwaves(Jakes & Cox, 1994). Microwave transmission is a very attractive transmission alternative for various applications. These applications range from the coverage of the rural, sparsely populated areas to the well-developed areas that require rapid expansion of telecommunications networks. Most of the commercially deployed terrestrial microwave point-to-point (also called radio-relay) systems use frequencies from approximately 2 to 60 GHz (and lately up to 90 GHz) with maximum hop lengths of around 200 km(Ali & Alhaider, 1992).

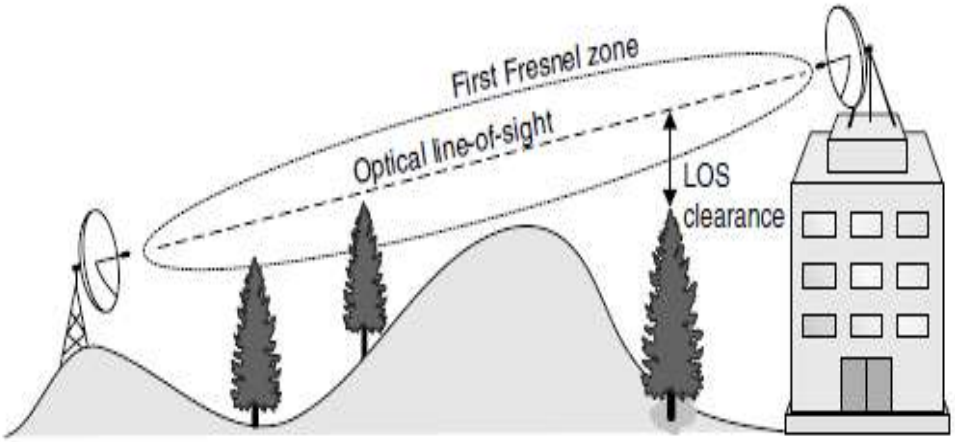

Figure 2.1: Optical and Radio Line of Sight (Ali & Alhaider, 1992).

Microwave point-to-point communications operate in a propagation mechanism similar to that of light propagation. Microwave radio communications require a clear path between parabolic antennas, commonly known as a line-of-sight (LOS) condition as seen in Figure 2.1. LOS exists when there is a direct path between two separate points having no obstructions (for example, buildings, trees, hills, or mountains) between them.

Radio waves propagation in free space or air occurs with acceptable loss while they are attenuated rapidly in sea-water or inside lands, increasing with frequency. Generally, every media of propagation is characterized by three parameters itemized as follows (Harb *et al.*, 2013):

i. Permittivity denoted by ϵ in Farad per meter (F/m)

ii. Permeability denoted byμ in Henry per meter (H/m)

iii. Conductivity denoted by σ in Siemens per meter (S/m)

In free space, values of the above parameters are:

$$\in_o = 8.85 \times 10^{-12} F/m$$

$$\mu_o = 4\pi x 10^{-12} H/m \text{ and}$$

$$\sigma = 0$$

where,

$\in_o$ is permittivity in free space,

μ_o is permeability in free space, and

σ is conductivity in free space.

2.3.1 Microwave Radio Applications

Microwave radio is used as a transport medium to facilitateinformation transmission in networks such as basic service networks, mobile cellular network, last mile access networks, private networks amongst others. Figure 2.2 shows the typical application of microwave application in GSM networks(Manning, 2009).

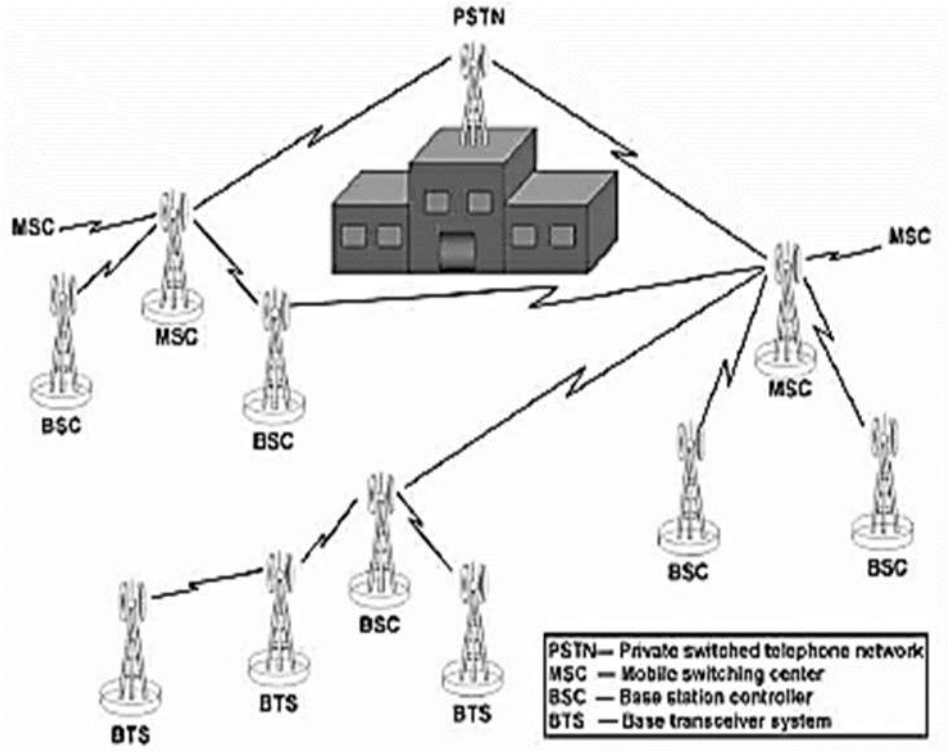

Figure 2.2: Microwave Application in a GSM Backhaul Network (Manning, 2009)

Microwave radio terminal has three basic modules which are as follows (Jakes & Cox, 1994):

i. **Digital Modem**: To interface with customer equipment and to convert customer traffic to modulated signal.

ii. **RF Unit**: To up and down convert signal in the RF Range.

iii. **Passive Parabolic Antenna**: For transmitting and receiving RF signal.

Given any two microwave station, the distance between them is called a hop. A hop can be exclusively explained as the portion of a signal's path from source to receiver. Figure 2.3 shows a pictorial representation of two microwave terminals forming a hop and thus, a microwave communication which requires line of sight (Manning, 2009).

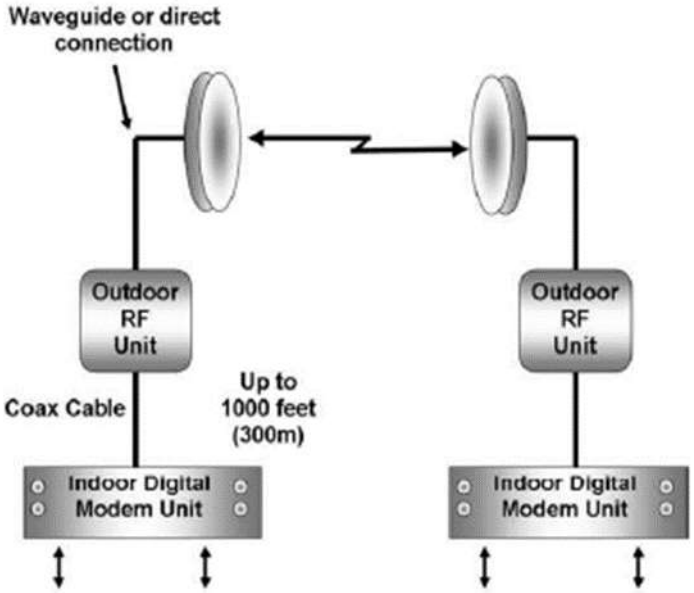

Figure.2.3: One Hop of Microwave Transmission (Manning, 2009)

In microwave transmission, frequency bands of 7GHz, 15GHz, 18GHz, and 23 GHz and 26GHz are allowed for deployment in the transport network by private operator based on the following (Rai, 2012):

i. 15 GHz, 18 GHz and 23 GHz, 26GHz bands are used for access network.
ii. 7 GHz band is used for backbone network.
iii. Different channelling plans are available in these bands to accommodate different bandwidth requirements.

For tropical regions like Nigeria, microwave transmission is operated within commercial frequencies of 7GHz, 15GHz, 18GHz,23Ghz and 26GHzwith a speculated future use of 35GHz and 38GHz (Kesavan *et al.*, 2012).

2.3.2 Transmission Losses in Radio Communication

Generally, radio waves propagating between transmitting and receiving antennas encounter transmission losses. These losses, in addition to free space loss, are subjected to excess attenuations, including the following items amongst others (Islam *et al.*, 2010)

i. RF feeder loss
ii. Propagation mechanisms losses
iii. Depolarization loss
iv. Losses due to precipitation (such as dust particles, raindrops, gaseous absorption etc.)

This research hereby focuses on the effect of losses which are due to precipitation (dust particle to be precise) on cross polarization of microwave access radio link.

2.4 Dust Particle Geometry

Dust is a composition of small particles having random irregular shapes without any specific symmetry and cannot be described by any simple geometry. The dust particle shape may vary from needle-like to almost perfect sphere or disc(Sharif, 2015). Dust particle shape is very complicated; the nearest geometry that approximates dust particle is the ellipsoid with axis ratio varying over wide range (from 0 to 1) as shown in Figure 2.4(Musa *et al.*, 2014a).

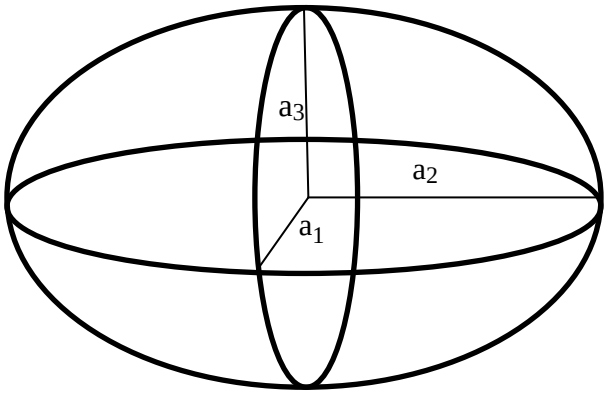

Figure 2.4: Ellipsoidal Model of Single Grain Dust Particle (Sharif, 2015).

The ellipsoid geometry has three degrees of freedom which give good approximation for the shape of realistic dust particles. The aspect ratios of the three axes a_1, a_2 and a_3 were

investigated and a ratio of the axis is found to be $1 : r_2 : r_3$ which corresponds to $1 : 0.71 : 0.53$ (Vyas *et al.*, 2014).

2.4.1 Particle Size Distribution

Particle sizes and distribution are important parameters both for investigating the characteristic properties of dust storm and calculating signal transmission parameters. The particle size distribution function affects the wave attenuation in dust storm. Attenuation and phase shift of a microwave signal have been estimated utilizing measured particle size distribution or numerical distribution methods. Unlike rain, there is paucity of data on dust particle sizes. Generally, the particle size distributions of dustare varied considerably and no clear pattern of prediction seems to be available (Sharif, 2015).

If the probabilityof finding particles with axis ratio between a_2 and a_1 in the range $r_{m-1} < r < r_{m+1}$ is $P_m(r)$ and the probability of the particles with axis ratio between a_3 and a_2 in the range $r_{n-1} < r < r_{n+1}$ is $P_m(r)$, then the probability of finding particles with and axes ratios within their respective ranges is $P_m(r)P_n(r)$ (Ghobrial & Sharief, 1987).

2.4.2 Particle Size Measurement Methods

The sizing methods involve both classical and modern instrumentations, based on a broad spectrum of physical principles. The typical measuring systems may be classified according to their operation mechanisms(Syvitski, 2007). The various methods used in measurement of particles are sieving, microscopy and sedimentation technique. Each of these methods have their advantages and disadvantages as shown in Table 2.1

Table2.1: Comparison of Particle Size Distribution Measurements Methods(Syvitski, 2007)

	Sieving	**Microscopy**	**Sedimentation**
Advantages	Easy to perform	Particles are individually examined	Required equipment can be relatively simple and impressive
	Wide range of sizes	Visual means to see sub-micron specimens	Can measure a wide range of sizes with accuracy and reproducibility
	Impressive	Particle shape can be measured	
Disadvantages	Problem of reproducibility	Very expensive	Large particles create turbulence, are slow and recorded as undersize
	Wear or damage when in use or clearing	Time consuming sample preparation	Careful temperature control is necessary to suppress convection currents
	Irregular/agglomerated particles	Materials such as emulsion are difficult to prepare	Particles have to be completely in the suspending liquid
	Labour intensive	Not suitable for routine use	The lower limit of particle size is set by the increasing importance of Brownian motion for progressively smaller particles

2.4.3 Dielectric Constant of Dust

The dielectric constant (or permittivity) of dust particle comprises two parts, which are the real part and the complex part. The real part of the relative permittivity of dust particles is an

important factor in determining depolarization and the imaginary part is a critical factor in the attenuation caused by the energy absorption. In turn, the moisture uptake is significant for the real part and critical for the imaginary part(Musa *et al.*, 2014b).

Microwave signal energy is lost in dust clouds through scattering, polarization loss, and absorption, all of which are created when dust particles in a volume of air change the electromagnetic properties of that volume. The net effect of mixing air and dust particles can be described by a dielectric mixing model(Wikner, 2008).

Since dust is a mixed material, the most accurate and popular formulae for effective permittivity is the Maxwell Garnett formula. The Maxwell Garnett formula for effective permittivity of a mixture in i direction, having suspended ellipsoidal particles with permittivity $\in_i$ suspended in a medium with permittivity $\in_a$ and particle having dielectric constant of $\in$ is given as (Sharif, 2015):

$$\in_i = \in_a \left[1 + V \frac{\in - \in_a}{\in_a + A_i (\in - \in_a)} \right] \tag{2.1}$$

where:

V is the volume of ellipsoidal particle in unit volume of storm

A_i is the depolarization factor along the *ith* axis for $i = 1,2,3,...$

2.4.3.1 Effect of Moisture Content on Dielectric Constant (Permittivity)

The dielectric property of water within mixtures is not the same as that of pure water because the ion content of water within mixtures is different. An example can be seen in Figure 2.5 where the exposure of water to silica dust particles promotes the ions transfer to water, which form an ionic halo around the particles(Liu *et al.*, 2013).

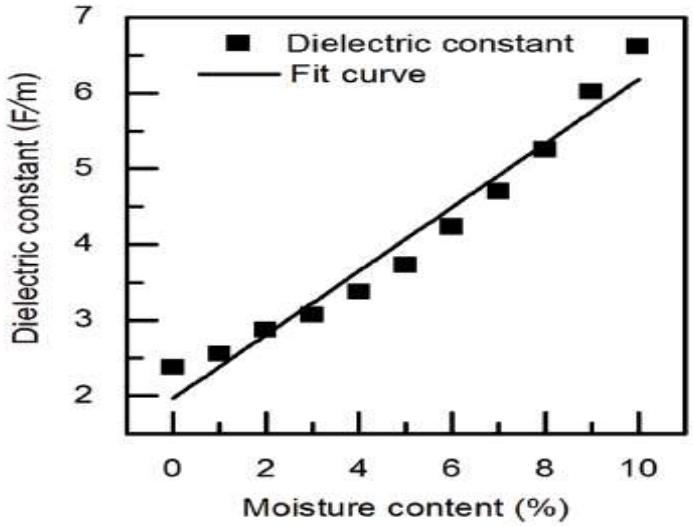

Figure 2.5: Variation of Dielectric Constant of Silica Dust Particles as a Linear Function of Moisture Content at 10 GHz(Liu *et al.*, 2013).

Hygroscopic water increases both real and imaginary parts of the dielectric constant. Water contents as low as 4.8% by weight cause the real part to increase by 48% and imaginary part by over 600% as observed in Figure 2.5. Chemical analysis shows that the major constituents of dust are SiO_2, Al_2O_3 and Fe_2O_3. Of these, SiO_2 is the major contributor to the real part while Al_2O_3 has the greatest effect on the imaginary part. The changes in both real and imaginary parts of the dielectric constant with frequency are small (Sharif, 2015).

2.4.3.2 Dielectric Constant for KanoRegion

Kano, which is a commercial city located in central northern Nigeria, records accumulations of 170-230 g/m^2/yr of dust (McTainsh, 1984). Thus, Kano area lies within the path of present-day dust plumes and on the humid margins of the Quaternary dune fields appear the most likely area of dust mantle formation (McTainsh, 1984).

David and Moses, (2011), presented a measurement of dielectric permittivity across Nigeria (Kano inclusive). In order to relate soil volumetric moisture content with relative dielectric permittivity,a simple formula can be used to obtain the relative dielectric permittivity which is given as(Topp *et al.*, 1980):

$$\in_a = 3.03 + 0.3\theta_v + 146\theta_v^2 - 76.7\theta_v^3 \qquad (2.2)$$

Where; θ_v is the soil volumetric content.

The graphical relationship between relative permittivity and volumetric moisture content for Kano region is shown in Figure 2.6 (David & Moses, 2011). From Figure 2.6, it can be seen that the graph follows the pattern of a cubic equation which is in conformity with the general formula for relative permittivity.

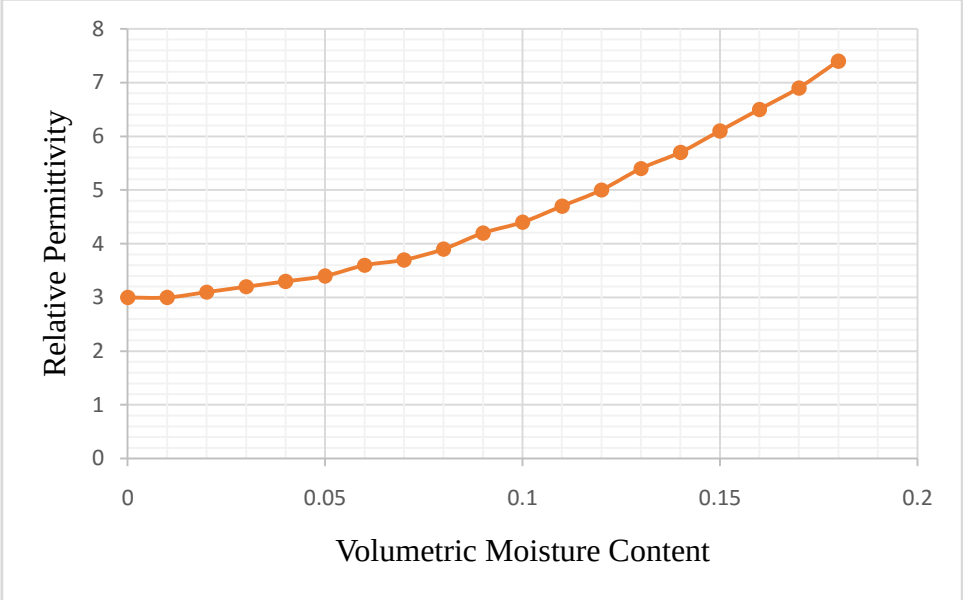

Figure 2.6: Permittivity Against Moisture Content (Kano Zone) (David & Moses, 2011)

2.4.4 Cross Polarization Discrimination Induced by the Atmosphere

In order to increase the line capacity of a given link without increasing the bandwidth of the signal, one generally resorts to orthogonal polarizations of either rectilinear or circular orientation. By using orthogonal polarizations, two independent information channels occupying the same radio frequency band can be transmitted over a single link. However, when a wave propagates through the atmosphere, a part of the energy emitted with a given polarization becomes orthogonally polarized, thereby causing interferences between the two communication channels (Bashir *et al.*, 2013).

While the orthogonally-polarized-channels are completely isolated in theory, some degree of interference between them is inevitable, owing to less-than-theoretical performance mobile station antennas, and depolarizing effects on the propagation path. The main sources of this

depolarization of wave frequencies are hydrometer absorption and scattering in the troposphere(Ghobrial & Sharief, 1987).

Depolarization is the phenomenon whereby all or part of a radio wave transmitted with a given polarization has no longer any defined polarization after the propagation. The phenomenon of trans-polarization is characterized by the appearance, during the course of propagation, of a polarization component (cross-polar component) orthogonal to the initial polarization (co-polar component) (Rai, 2012).

2.4.4.1 Cross and Co-polarization

A measure of the degree of interference between the two orthogonally-polarized channels is the Cross Polarization Discrimination which is simply denoted as XPD(Sharif, 2015). For example, letE_{ij}be the magnitude of the electric field at the receiver that is transmitted in polarization state i and received in the orthogonal polarization state j (i,j=l,2). Hence E_{11}, E_{22}denote the co-polarized waves and E_{21}, E_{12}refer to the cross-polarized waves as shown in Figure 2.7.

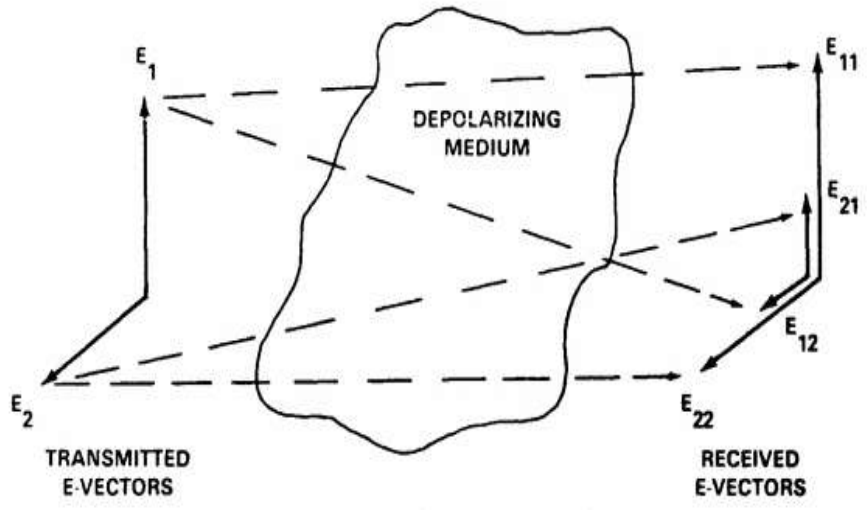

Figure 2.7: Co-Polarized and Cross Polarized Wave (Sharif, 2015)

XPD is the ratio (in dB) of the power in the co-polarized wave to the power in the cross-polarized wave that is transmitted in the same polarization state (Sharif, 2015).

$$XPD = 20\log\frac{E_{11}}{E_{21}} \tag{2.3}$$

2.4.5 Analytical Methods to Single Particle Scattering

The analytical method is the use of conventional mathematical solutions of Maxwell's equations for the scattering of electromagnetic waves by dielectric particles. Thesemethods include the Rayleigh approximation method and the Mie theory (Islam *et al.*, 2010).

2.4.5.1 Rayleigh Approximation Method

The Rayleigh approximation scattering is about the simplest approximation method. It is a function of electric polarizability of particles and occurs when the particle is electrically small. However, once the particle is of the order of the size of the wavelength, Mie scattering occurs (Sharif, 2015). The assumption for Rayleigh approximation is that $k < 1$

$$k = \frac{2\pi}{\lambda} \tag{2.4}$$

where:

k is the wave number,

λ is the wavelength

In the Rayleigh approximation, the field inside the scattering particle is not modelled properly. For an exact solution the scattered field reflects all the properties of the object which is no longer true for an approximation solution. The total cross-section efficiency factor is expressed as (Sharif, 2015):

$$\sigma_t = \left[\frac{8}{3}\pi a^2\left(ka^4\right) + 12\pi a^2(ka)\frac{\varepsilon''}{\left(\varepsilon'-1\right)+\left(\varepsilon''\right)^2}\right]\left|\frac{\varepsilon-1}{\varepsilon+2}\right|^2 \tag{2.5}$$

where:

a is the particle radius,

k is the wave number,

$\varepsilon' and \varepsilon''$ are the real and imaginary relative dielectric constants of the particles.

2.4.5.2 Mie Theory

Mie theory unlike that of Rayleigh, gives a complete analytical solution of the Maxwell's equations. The solution accommodates possible ratios of particle diameter and wavelength. The extinction or total cross-section efficiency factors by Mie solutions can be expressed as (Sharif, 2015):

$$\sigma_t = \frac{\lambda^2}{2\pi}(ka)^3[c_1 + c_2(ka)^2 c_3(ka)^3] \tag{2.6}$$

where, C_1, C_2 and C_3 are constants whose values depend on $\varepsilon' and \varepsilon''$ defined as:

$$C_1 = \frac{6\varepsilon''}{(\varepsilon'+2)^2 + \varepsilon''^2} \tag{2.7}$$

$$C_2 = \varepsilon''\left\{\frac{6}{5}\frac{7\varepsilon'^2+7\varepsilon''^2+4\varepsilon'-20}{\left[(\varepsilon'+2)^2+\varepsilon''^2\right]} + \frac{1}{15} + \frac{5}{3\left[(2\varepsilon'+3)^2+4\varepsilon''^2\right]}\right\} \tag{2.8}$$

$$C_3 = \frac{4}{3}\left\{\frac{(\varepsilon'-1)^2(\varepsilon'+2)+\left[2(\varepsilon'-1)(\varepsilon'+2)-9\right]+\varepsilon''^4}{\left[(\varepsilon'+2)^2+\varepsilon''^2\right]^2}\right\} \tag{2.9}$$

The Mie theory application is limited to spherical particles only but do not depend upon any such limitation and can be utilized to predict attenuation in microwave wave band with high reliability, especially at higher frequencies used by new systems with larger bandwidth.

2.4.6 Dust Storm Depolarization

Depolarization of dust storm involves the depolarization of microwave propagation through atmosphere having dust particles of ellipsoidal shape. When a linearly polarized wave incidents on a non-spherical dust particle at an angle ofθ, the electric vector of the wave can be resolved into two components and along the OX and OY axis as shown in Figure. 2.8.

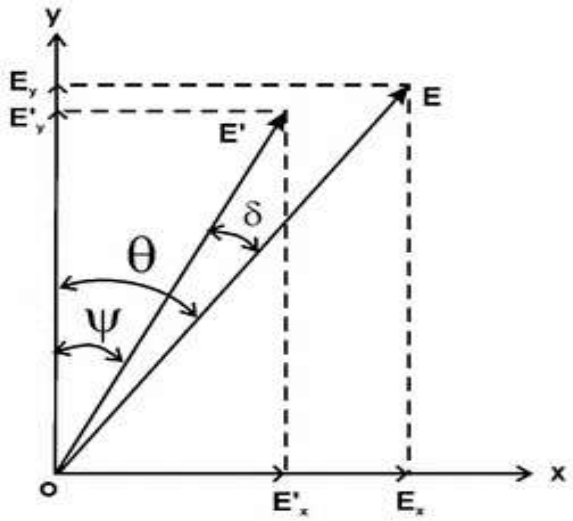

Figure 2.8: Relationship between Incident Canting Wave E and Depolarized Wave E'(Rai, 2012).

$$E = E_x i + E_y j \tag{2.10}$$

Thus, i and j are unit vector component on the OX and OY respectively where,

$$E_x = E \sin\theta \cos\omega t \tag{2.11}$$

and

$$E_y = E \cos\theta \cos\omega t \tag{2.12}$$

Furthermore, if $\alpha_x \; and \; \alpha_y$ are the attenuation factors and $\beta_x \; and \; \beta_y$ are the phase constant along OX and OY axes respectively, depolarized wave vector may be expressed as:

$$E' = E'_x \, i + E'_y \, j \tag{2.13}$$

where:

E_x is the electric field of the OX axis,

E_y is the electric field of the OY axis,

E'_x is the depolarized field in the OX axis,

E'_y is the depolarized field in the OY axis,

Given that attenuation along OX and OY axes as $e^{-\alpha_x L}$ and $e^{-\alpha_y L}$ and phase shift along respective axes are expressed as $\beta_x L$ and $\beta_y L$, therefore components $E_x^{'}$ and $E_y^{'}$ can be expressed as (Rai, 2012):

$$E'_x = E\sin\theta e^{-\alpha_x L}\cos\left[\omega t - \beta_x L\right] \tag{2.14}$$

$$E'_y = E\cos\theta e^{-\alpha_y L}\cos\left[\omega t - \beta_y L\right] \tag{2.15}$$

Where;

L is the distance,

Ω is the angular frequency and

t is time

In this case, if differential attenuation is considered to be the major cause of depolarization produced by dust particles, then the effect of differential phase shift can be considered negligible such that(Rai, 2012):

$$\left[\beta_x - \beta_y\right]L = 0 \xrightarrow{yields} \beta_x L = \beta_y L \tag{2.16}$$

From Figure 2.8, it can be obtained that:

$$\tan\psi = \frac{E'_x}{E'_y} \tag{2.17}$$

Substituting equations (2.14) and (2.15) into equation (2.17), this gives:

$$\tan\psi = \frac{E\sin\theta e^{-\alpha_x L}\cos\left[\omega t - \beta_x L\right]}{E\sin\theta e^{-\alpha_y L}\cos\left[\omega t - \beta_y L\right]} \tag{2.18}$$

Substituting equation (2.16) into (2.18) gives $\tan\psi$ as:

$$\tan\psi = \tan\theta e^{-(\alpha_x - \alpha_y)L} \tag{2.19}$$

$$\psi = \tan^{-1}\left[\tan\theta e^{-(\alpha_x - \alpha_y)L}\right] \tag{2.20}$$

$$e^{-(\alpha_x-\alpha_y)L} = \log_{10}^{-1}\left[\frac{-(\alpha_x-\alpha_y)L(dB)}{20}\right] \tag{2.21}$$

Where α_x, α_y are in dB/km and L in km.

Substituting equation (2.21) into equation (2.20) gives ψ as:

$$\psi = \tan^{-1}\left[\tan\theta \log_{10}^{-1}\left[\frac{-(\alpha_x-\alpha_y)L(dB)}{20}\right]\right] \tag{2.22}$$

Therefore, it can be seen from Figure 2.8 that due to differential attenuation the incident linearly polarized vector is rotated by an angle while passing through the medium and attains the resultant electric vector amplitude. It is, therefore, clear that the depolarization angle is given by(Rai, 2012):

$$\delta = \theta - \psi \tag{2.23}$$

$$\delta = \theta - \tan^{-1}\left[\tan\theta \log_{10}^{-1}\left[\frac{-(\alpha_x-\alpha_y)L(dB)}{20}\right]\right] \tag{2.24}$$

Finally, XPD can be given as(Rai, 2012):

$$XPD(dB) = 20\log\left[\frac{\sin\delta}{\cos\delta}\right] \tag{2.25}$$

$$XPD(dB) = 20\log(\tan\delta) \tag{2.26}$$

From equations (2.25) and (2.26), it may be noted that to find the value of depolarization, the attenuation factors must be known.

2.4.6.1 Visibility

Knowledge of visibility has guided the formulation of propagation models in dust storm. It is a more realistic parameter that meteorological observations of dust storms are usually based

upon. Optical visibility is directly related to the severity of dust storms and thus a measure of the severity of the storm. Visibility is often used to describe the distance at which a mark disappears against the background for terrestrial dust storm. The term visibility is also normally applied to denote the degree of dust storm density instead of the total number of dust particles. Needless to mention that visibility decreases with increasing intensity of dust in a storm. Low visibility implies high number concentration of particles while low number concentration of particles represents high visibility. A measure of the severity of a dust storm is visibility, which decreases with increasing number of particles in the atmosphere (Musa *et al.*, 2014a).

The mass of suspending dust per unit volume of air is related to visibility as seen in the equation (2.27) (Saleh & Abuhdima, 2011):

$$M = \frac{C}{v^{\gamma}} \tag{2.27}$$

Where;

M is the dispersed density in the medium (dust mass concentration) in Kg/m^3

v is the Visibility (km)

C and γ are constants that depend on the type of land from which the storm originated as well as the climatic conditions.

There is no single value of *C* that is generally applicable to relate the mass concentration of soil-derived aerosols and visibility. Different values have been reported in the literature (Musa *et al.*, 2014b).

When solid density ρ_0 is considered, equation (2.27) becomes:

$$V_r = \frac{M}{\rho_0} \tag{2.28}$$

Substituting the mass (M) in equation (2.28) gives:

$$V_r = \frac{C}{\rho_0 V^{\gamma}} \tag{2.29}$$

where;

V_r is the Relative dust volume in air,

C *and* γ are constants,

v is the visibility,

ρ_o is the relative density of air.

2.4.6.2 Dielectric Constant

The best technique used to obtain the dielectric constant of dust in any particular area at different frequency bands is by measurement under experimental conditions. It has already been established that moisture content of dust seriously increases the dielectric constant of dust. The most reasonable and accurate values of dielectric constants for each frequency band is shown in Table 2.2. However, the values of dielectric constant can also be obtained using known or measured relative humidity values which can be computed as follows (Sharif, 2015):

$$\in_H^{'} = \in^{'} + 0.04H - 7.78\times10^{-4}H^2 + 5.56\times10^{-6}H^3 \tag{2.30}$$

$$\in_H^{''} = \in^{''} + 0.02H - 3.71\times10^{-4}H^2 + 2.76\times10^{-6}H^3 \tag{2.31}$$

where; $\in^{'} + j \in^{''}$ are the values of dry dust dielectric constants.

Table 2.2: Dry Dust Dielectric Constants (Sharif, 2015)

Band	Frequency Range (GHz)	Dielectric Constant
S	2-4	4.56+j0.251
X	8-12	5.73+j0.415
Ku	12-18	5.5+j1.300
K	18-26.5	5.1+j1.400
Ka	26.5-40	4.00+j1.325
W	56-100	3.50+j1.640

2.4.6.3 Dusty Medium Permittivity

The permittivity of a dusty medium can be obtained using the Maxwell Garnett formula shown in equation (2.1). Since the dust particles are assumed to be approximately ellipsoidal in nature, the dipole moment induced on the dust particle depends on the direction of the electric field that excite the particle. Thus, the dust medium is classified as an isotropic medium in which the permittivity depends on the direction considered. Given an effective permittivity of dust mixture $\in_{\vartheta,i}$, the following can be obtained (Sharif, 2015):

$$\in_{\vartheta,i} = \in_a \left\{ 1 + v \frac{\in - \in_a}{\in_a + A_i (\in - \in_a)} \right\} \tag{2.32}$$

where:

v is the volume of the dust particle,

A_i is the depolarization factor in the i-direction,

$\in$ is the permittivity of the dust particle suspended in a medium,

$\in_a$ is the permittivity of the medium which is air.

For a medium of air, $\in_a$ has a value which is equal to one (1), thus equation (2.32) can be re-written as:

$$\in_{\vartheta,i} = \in_a \left\{ 1 + \nu \frac{\in -1}{1 + A_i (\in -1)} \right\} \tag{2.33}$$

$$\in_{\vartheta,i} = 1 + \xi_i \tag{2.34}$$

where; $\in_{\vartheta,i} = 1 + \xi_i$ is the normalized polarizability (that is, the ability of the particles to acquire a dipole moment in an electric field), divided by the volume and permittivity of free space.

2.4.6.4 Wave Attenuation in a Lossy Medium

For a lossy medium, electromagnetic fields must always satisfy Maxwell's equations assuming sinusoidal time dependence. To evaluate the attenuation factor for horizontal and vertical polarizations it is necessary to consider the value of propagation constant in a lossy dielectric medium. The wave equation is given by(Hong *et al.*, 2008):

$$\nabla^2 E - \gamma^2 E = 0 \tag{2.35}$$

Having a solution such that:

$$E = |E| e^{\gamma z} e^{-i\omega t} \hat{z} \tag{2.36}$$

$$\gamma = \alpha + i\beta = j \frac{\omega}{c} \sqrt{\in} \tag{2.37}$$

where:

α is the attenuation,

β is the phase shift

ω is the frequency

c is the speed of light,

ϵ is the dielectric constant of the medium (that is, suspended dust particle)

$\hat{z}$ is a unit vector orthogonal to plane XY as shown in Figure 2.8

Given that N dust particles are contained in volume V, the propagation constant of the EM wave facing the i^{th} direction.

$$\gamma_P = \alpha_i + i\beta_i = j\frac{\omega}{c}\sqrt{\epsilon_i} \tag{2.38}$$

where:

ϵ_i is the effective dielectric constant of the medium having suspended dust

Since,

$$\epsilon_i = 1 + \frac{V(\epsilon - 1)}{1 + A_i(\epsilon - 1)} \tag{2.39}$$

Then, equation (2.38) becomes:

$$\gamma_P = \alpha_i + i\beta_i = j\frac{\omega}{c}\left[1 + \frac{V(\epsilon - 1)}{1 + A_i(\epsilon - 1)}\right]^{\frac{1}{2}} \tag{2.40}$$

Now neglecting the higher power terms in the expansion for a very small value of *V*, equation (2.40) gives:

$$\gamma_P = j\frac{\omega}{c}\left\{1 + \frac{V(\epsilon - 1)}{2[1 + A_i(\epsilon - 1)]}\right\}^{\frac{1}{2}} \tag{2.41}$$

Equating the real and imaginary parts and taking into consideration the equation of speed which is(Bashir *et al.*, 2013):

$$c = f\lambda \tag{2.42}$$

Hence, α_i and β_i can be obtained as (Sharif, 2015):

$$\gamma_P = j\frac{\omega}{c}\left\{1+\frac{V(\in -1)}{2[1+A_i(\in -1)]}\right\}^{\frac{1}{2}} = j\frac{2\pi}{\lambda}\left\{1+\frac{V(\in -1)}{2[1+A_i(\in -1)]}\right\}^{\frac{1}{2}} \tag{2.43}$$

Thus,

$$\alpha_i = -\frac{\pi}{\lambda}\,\mathrm{Im}\left[\frac{V(\in -1)}{1+A_i(\in -1)}\right]^{\frac{1}{2}} \tag{2.44}$$

and

$$\beta_i = \frac{2\pi}{\lambda}\left[1+\mathrm{Re}\,\frac{V(\in -1)}{1+A_i(\in -1)}\right]^{\frac{1}{2}} \tag{2.45}$$

The attenuation along axes 1, 2, and 3 can be estimated utilizing measured Particle Size Distribution (PSD) as follows (Ghobrial & Sharief, 1987):

$$\alpha_{1,m,n} = -\frac{\pi}{\lambda}\sum_n VP_m P_n\left(\frac{1}{A_{1,m,n}+\frac{1}{\in -1}}\right) \tag{2.46}$$

$$\alpha_{2,m,n} = -\frac{\pi}{\lambda}\sum_n VP_m P_n\left(\frac{1}{A_{2,m,n}+\frac{1}{\in -1}}\right) \tag{2.47}$$

$$\alpha_{3,m,n} = -\frac{\pi}{\lambda}\sum_{n} VP_m P_n \left(\frac{1}{A_{3,m,n} + \frac{1}{\in -1}} \right) \tag{2.48}$$

where:

P_n is the probability of finding dust particle with a_3/a_2 axis ratio in the range.

$r_{n-1} < r < r_{n+1}$ and,

P_m is the probability of finding dust particle with a_2/a_1 axis ratio in the range,

$r_{m-1} < r < r_{m+1}$.

2.4.6.5 Dusty Media Depolarization Factor

Given an ellipsoidal geometry of a dust particle as shown in Figure 2.4, where the semi axes fall in the order, and are orthogonal in directions, the depolarization factor in the i^{th}direction is given as follows (Sharif, 2015):

$$A_i = \frac{a_1 a_2 a_3}{2}\int_0^{\infty} \frac{1}{\left(s + a_i\sqrt{(s+a_1)(s+a_2)(s+a_3)}\right)} \tag{2.49}$$

However, according to equivalent medium theory, dust particles can be equivalent to homogeneous medium in which the radius of all particles are the same. Therefore, the depolarization factor in the three axes of a_1, a_2 and a_3 are 0.243, 0.324 and 0.432, respectively (Sun *et al.*, 2013).

For a vertically polarized wave, the direction of the electric field is parallel to the shortest axis of the precipitating particle on the OY axis (which can be given as(Musa *et al.*, 2014a):

$$\alpha_y = \alpha_3 = \alpha_{3,m,n} = -\frac{\pi}{\lambda}\sum_n VP_m P_n \,\mathrm{Im}\left(\frac{1}{A_{3,m,n} + \frac{1}{\in -1}}\right) \tag{2.50}$$

Similarly, the propagation constants for horizontal polarization on OX axis (are obtained following the same analysis as for vertical polarization. However, in thiscase the subscript 3is replaced by either 1 or 2. Since the particles have no particular orientation in the horizontal plane, the attenuation and phase shift constants are obtained as follows (Musa *et al.*, 2014b):

$$\alpha_x = \frac{\alpha_1 + \alpha_2}{2} = -\frac{\pi}{2\lambda}\sum_n VP_m P_n \,\mathrm{Im}\left(\frac{1}{A_{1,m,n} + \frac{1}{\in -1}} + \frac{1}{A_{2,m,n} + \frac{1}{\in -1}}\right) \tag{2.51}$$

In conclusion, the value of the Cross Pole Discrimination (XPD) whose equation is presented as equation (2.25) can be obtained based on the following:

i. Computation of the horizontal plane attenuation, α_X,
ii. Computation of the vertical plane attenuation, α_Y,
iii. Computation of the differential attenuation, $\alpha_x - \alpha_y$
iv. Finally, XPD values can be obtained.

2.4.6.6 Loss Due to Depolarization

In order to obtain the loss due to depolarization in medium having sand of dust particles, E_1 can be considered as the incident field. After passing through the medium, the polarization plane of the incident wave changes such that if the medium produces the depolarization of an angle, δ then the effective values of electric field after passing through the medium will be E_1 multiplied by the cosine of parallel to the medium having dust particles. This can be used to obtain the loss due to polarization (L_d) as follows (Rai, 2012):

$$L_d = \frac{E_1^2 - E_2^2 \cos^2 \delta}{\eta_o} \tag{2.52}$$

where, η_0 is the intrinsic impedance of the free space medium.

Thus,

$$L_d = 10\log\left(\frac{1}{\cos^2 \delta}\right) \tag{2.53}$$

Substituting $\delta$from equation (2.24) into equation (2.53) gives:

$$L_d = 10\log\left(\frac{1}{\cos^2\left\{\theta - \tan^{-1}\left[\tan\theta \log_{10}^{-1}\left[\frac{-(\alpha_x - \alpha_y)L(dB)}{20}\right]\right]\right\}}\right) \tag{2.54}$$

2.4.7 Microwave Link Budget

When a wave signal is travelling along different paths thereby causing interference with other waves travelling on the direct line-of-sight path, multipath fading is said to occur. Hence, waves travelling along different paths end up completely out of phase and cancel each other. The fading problem isresolved by having enough fade margin which is factored into the link budget to overcome this loss when designing a wireless system. The amount of fade margin required depends on the desired reliability of the link but it is always advisable to maintain a fade margin of between 20dB to 30dB at all times. The percentage time availability of a link can be deduced using the Rayleigh fading model such that each value of fade margin gives a specific percentage time availability as shown in Table 2.3.Fade margin is calculated as follows(Tranzeo, 2010):

$$Fade\ M\arg in(dB) = received\ Power - receive\ Sensitivity \tag{2.55}$$

Where; receive sensitivity is constant for the desired kind of antenna and the received power is obtained as follows:

$$\text{Re}\,ceived\ Power = Tx\ Power + Gains - Losses \tag{2.56}$$

Table 2.3: Link Availability Based on Rayleigh Fading Model(Freeman, 2005)

Time Availability (%)	**Fade Margin (dB)**
90	8
99	18
99.9	28
99.99	38
99.999	48

If the gains are those of transmitter (Tx) and receiver (Rx) antenna gains and the loss is Free-Space Path Loss, then equation (2.56)is re-written as:

$$\text{Re}\,ceived\ Power = Tx\ Power + Tx\,Gain + Rx\,Gain - FSPL \tag{2.57}$$

The Free-Space Path Loss (FSPL) is then obtained as follows:

$$FSPL = 20\log_{10}(d) + 20\log_{10}(f) + 32.45 \tag{2.58}$$

where:

d represents the distance between the transmitter and receiver

f is the frequency of the signal.

Thus, equation (2.55) can also be written as:

$$Fade\ M\arg in = Tx\,Power + Tx\,Gain + Rx\,Gain - FSPL - receive\,Sensitivity$$

(2.59)

2.4.8 Eclipse Radio Datasheet

In order to validate the model developed in this research, the eclipse ODU300HP radio is selected. The parameters of this radiois used to design a link budget template based on XPD degradation for Kano. The parameters of the radio are illustrated in Table 2.4.

Table 2.4: Parameters of Eclipse ODU300HP Radio(Eclipse, 2015)

Frequency	**18GHz**	**23GHz**	**26GHz**	**28GHz**	**32GHz**
Tx Power(dBm)	16.5	16.5	12.5	15	15
Tx Antenna Gain (dB)	88	87.5	82	83.5	83
Rx Antenna Gain (dB)	88	87.5	82	83.5	83
Receive Sensitivity (dBm)	-71.5	-71	-69.5	-69	-68.5

Table 2.4 shows the data for different frequencies of the specified radio at a bandwidth of 200Mbps. These parameters can be used to obtain the value of received power when performing a wireless link budget analysis.

2.5 Review of Similar Research Works

This section deals with the review of previously published research works that are considered to be directly relevant and critical to this research. It is from these reviews that the extent of research in this area will be known and what achievements and contributions have been made. However, the following are some of the relevant literatures reviewed.

Elshaikh *et al.*, (2009) developed a mathematical model to predict the signal attenuation due to dust storm. The model was used to calculate the signal path attenuation based on Mie

solution of Maxwell's equation. The model enabled a convenient calculation of the microwave signal path attenuation which related attenuation to visibility, frequency, particle size and complex permittivity. The proposed mathematical model showed that the microwave signal attenuation due to dust storm depended on visibility, frequency, dust particle radius and dielectric constant. There were directly proportional relationships between the attenuation values and the frequency, dust particle radius and dielectric constant, while it had inverse proportional relationship to visibility values. The predicted values from the mathematical model, which were compared with the measured values observed in Saudi Arabia and Sudan showed relatively optimistic agreement. However, the proposed mathematical model, did not take in to account effect of moisture content in these areas as reported by other authors.

Islam *et al.,* (2010) developed a model to predict microwave attenuation due to dust particles using Mie solution of Maxwell's equations for the scattering of electromagnetic wave. The predictions showed that the attenuation varied from 13dB/km to 0.2dB/km at 40GHz for dust particle radius equal to 50μm and the visibility varied from 10m to 500m. At higher frequency of 100GHz, the attenuation varies from 47dB/km to 2dB/km for dust particle radius equal to 50μm and the visibility varied from 10m to 500m. The predicted values from the mathematical model were compared with the measured values observed in Saudi Arabia and Sudan. The proposed model predicted the measured data more accurately than existing model. The accurate prediction was useful to design higher frequency links at areas affected by dust storms. Though moisture content was not taken into consideration.

Dong *et al.,* (2011) carried out quantitative studies on the attenuation and phase delay caused by dust storms using "effective material technique and general formulation complex propagation factor". The analysis took into account multiple scattering effects in the

computation of attenuation, a factor which was not considered were the scattering theories (Rayleigh scattering approximation and Mie scattering theory). Attenuation at different frequencies was calculated and their values were validated with the ones obtained from Raleigh scattering. From the results presented, it was established that attenuation dropped dramatically with the increase in visibility and that the attenuation is insignificant except for very high frequencies (above 30 GHz) as well as for very dense storms. The results also revealed that for a propagation path of over 1 km having a visibility of 10m, there might be tendency of severe cross-polarization, which could lead to a signal loss in microwave and millimetre-wave links. However, extra work needs to be done in order to precisely compute the complex permittivity of dust particles mixing with air and water so that a precise model of dust storms with respect to signal attenuation and phase delay is obtained.

Saleh and Abuhdima, (2011) investigated the effect of dust storms on wireless communication, such as microwave links (15 GHz to 26GHz), in the southern region of Libya (Sebha, Ashati, Obari, Morzok, Ghat) by determining the attenuation. The author carried out analysis for samples such as particle size distribution, average density and chemical composition, which were used to compute the dielectric constant and attenuation factors. Calculation of average density and complex permittivity of samples in Southern region were equal to 2.5764gm/m^3, 6.3485-j0.0929, respectively and the attenuation constant of the region of study was equal to 0.2412dB/km where weather conditions due to dust storms were described as visibility equal to 4m (worst case) and humidity equals to 0 percent, 60 percent and 100 percent at any height. However, the lesser accurate Looyenga equation was used to calculate dielectric constant of mixture of air, water and dust instead of the Maxwell Garnett's equation that is a more accurate model for evaluating dielectric constant of mixture.

Musa and Bashir, (2013) investigated effects of dust storms on propagation of electromagnetic wave at millimetre wave band. Raleigh method was used to develop a formula for attenuation based on the complex forward scattering amplitude of spherical dust particles. The model showed that attenuation and phase shift were found to be dependent on visibility, wavelength and complex permittivity. They were also observed to be dependent on the moisture content of the dust particles in the storms. The geometry of the particle was assumed uniform for all particles that is all particles were spheres of the same radii.However, more recent research articles reveal that dust particles could best be approximated as spheroids, and furthermore,recent authors validated that particle geometry and size distribution were significant factors that affected attenuation in dust storms. These researches disqualified Musa and Bashir, (2013) research.

Bashir *et al.*, (2013)conducted a research work on the effect of propagation of electromagnetic waves through dusty particles for quantifying some telecommunication channel impairments. Rayleigh scattering theory was used to compute the Cross-Polarization Discrimination (XDP) for different sizes of dust storm particles. The results of the computation were compared with the solutions obtained from Maxwell's main equations using a Point Matching Technique (PMT) and it showed a strong correlation between Rayleigh approximations and PMT. The XPD values were computed at frequency bands of 12 GHz to 18GHz. The author compared an analytical method (Raleigh scattering) to a numerical method (PMT) where similar assumptions were made and similar results were obtained from both methods. However, when the two analytical methods (Raleigh and Mie scattering) were compared there was deviation in results due to the fact that Mie technique provided full solution to Maxwell's equation eliminating assumptions made by Raleigh. Thus the use of Mie technique disqualified Bashir *et al*.,(2013) as being not perfect.

Musa *et al.*, (2014b) investigated the Cross Polarization Discrimination (XPD) induced by dust storms at millimetre wave band. The work introduced simple models of wave propagation through dust storms. The models were developed based on the forward scattering amplitude of dust particles using Rayleigh method. It was observed that the phase shift and the signal attenuation caused by dust storm vary directly with the frequency and dielectric constant but were inversely proportional to the visibility. During severe dust storms, attenuation became significant but negligible as the visibility increases. Rayleigh scattering could be used to predict the losses at lower frequency side of the millimetre wave band. However,the assumption of forward scattering amplitude of dust particle is insufficient in the modelling of dust particle as this does not fully capture the effect of dust particle in air.

Sharif, (2015) investigated the electrical and mechanical properties of dusty media needed to study the propagation of microwave signals in such media. The parameters which were considered in this paper included

(i) The dust particle geometry which was approximated as an ellipsoid

(ii) Its orientation when suspended in air and the dust particles particle size distribution which was found to follow power law.

(iii) Visibility statistics during dust storms as observed in some towns in Sudan, and its variation with height, permittivity and depolarization factor of the dusty medium.

The permittivity and depolarization factor were derived based on Maxwell Garnett formula and dusty media propagation constant and phase shift were used to estimate signal attenuation and cross depolarization. The author concluded that depolarization factor computation involved solution of the first and the second kind Elliptic integral hence the computation of the dusty media depolarization and permittivity was not simple and it needed

some efforts. Numerical computations were evaded in this paper because the author highlighted the difficulties involved in the computation of cross depolarization. Secondly,the author observed power square law was best fit for particle size distribution. However, several literatures have proven that the log normal distribution is the best model to represent particle size distribution. This is because power square law is an inaccurate curve fitting model associated with a high error value thus the research is guaranteed to have high modelling errors.

Bilal *et al.*, (2015)investigated the impacts of dust storms with respect to the polarization conditions of microwave signal. The depolarization model described was used to compute the differential attenuation and phase shift for the six microwave bands (S, X, Ku, K, Ka and W). The polarization indices were computed for different axial ratios and visibilities in the presence of moisture for 0%, 5% and 10% relative humidity values. Results suggested that induced differential attenuation and differential phase shift were high when axial ration of particles were too small and visibility was low. It was found that differential attenuation was more sensitive to relative humidity than differential phase shift particularly for low frequency bands. Higher frequency bands were more depolarized by dust particles than low frequency bands. However, formulae for horizontal and vertical complex propagation constants of the medium referenced as basis for research were not verifiable. Graphs showing relationship between differential attenuation and phase shift with respect to frequency, relative humidity, and visibility were captured, however graphs of Cross Pole Discrimination (XPD) with regards to variables highlighted earlier were not captured as it was the key parameter in this research area.

In conclusion different researches that investigated the behaviour of microwave propagation through dust storms have been critically reviewed. The parameters such as attenuation, phase

shift, cross pole discrimination have been of great interest to the authors because they are key microwave signal quality parameters in line of sight propagation. These parameters are heavily dependent on variables like visibility, frequency, dielectric constant, particle size distribution, moisture content of medium. There were limitations in each of the reviewed researches, in the sense that some of these variables were not taken into consideration or not analysed in details. Forexample, most of the authors neglected the effect of moisture content while some used simple geometry for particle geometry. Hence, in this research every variable that typically affects the propagation of microwave signal operating with a dual polarization in dust storms is taken into consideration.

Also, most of the literatures consulted based their studies on either temperate region like Europe or the Asian peninsular, where the design of microwave links are restricted to these areas. More research work in this area is needed to be done in order to addressthe effect of dust storm in many parts of Africa severely affected by these factors. This will lead to the evolution of home based technologies that could be deployed to resolve such problems. Based on the forgoing, this research work will seek to address some of the highlighted loop holes associated with the works reported therein with particular attention to the peculiarities in the North West of Nigeria, with Kano as a focal point.

CHAPTER THREE

METHODOLOGY

3.1 Introduction

This Chapter presents the step by step procedure of the methodology used in achieving the aim and objectives of this research. It also gives full account of how the research work was carried out in order to obtain the desired results.

3.2 Methodology

The following steps make up the methodology followed to achieve the objectives:

i. Solving Maxwell's electromagnetic equation in the random medium (dust storm medium) to deduce complex propagation coefficients (attenuation and phase constant) as functions of variables including wave frequency, media dielectric constant, depolarization factor, and fractional volume of dust particle.

ii. Deduction of the mathematical relationship between visibility and fractional volume of dust particle.

iii. Using meteorological data (Kano) to deduce dielectric constant.

iv. Establishing:

   a. Probability distribution function from particle size distribution data,

   b. Mathematical relationship between XPD as a function of signal frequency, dielectric constant of dust storm, particle size probability distribution function and visibility at foremost.

v. Deduction of the fade Margin due to wave depolarization of a co-channel dual polarized microwave transmission link

vi. Modelling and programming of attenuation and XPD data against visibility data using MATLAB R2015b and validation of the results.

3.3 Data Collection

Meteorological data for a period of ten years (2003-2012) was obtained from Nigerian Meteorological Agency (NIMET) as shown in Appendix A1, A2, B1, and B2. The data collected included dust mass concentration, visibility, relative humidity, and particle size distribution for Kano. Tables 3.1 and 3.2 show the extracted data of visibility and relative humidity respectively, during the significant harmattan periods (i.e. October to February).

Table 3.1: Extracted Monthly Visibility Average for Harmattan Period in Kano

Year	**October(m)**	**November(m)**	**December(m)**	**January(m)**	**February(m)**
2003	190	290	1590	280	1790
2004	1500	280	290	260	570
2005	1640	1440	140	160	3430
2006	5120	150	160	1620	2260
2007	140	130	230	220	1720
2008	3260	1390	100	1430	450
2009	100	200	100	200	1580
2010	100	100	100	110	3550
2011	150	120	100	120	2350
2012	100	100	1190	1800	300
Average	1230	420	400	620	1800

Table 3.1 shows the monthly visibility values of harmattan period for a duration of ten years in Kano and its corresponding monthly average while Table 3.2 shows the same data set for percentage humidity.

Table 3.2: Extracted Monthly Humidity Average Values for Harmattan Period in Kano

Year	October(%)	November(%)	December(%)	January(%)	February(%)
2003	59	33	29	29	27
2004	57	33	31	32	28
2005	62	36	30	32	27
2006	55	37	33	30	25
2007	60	38	31	31	28
2008	60	34	32	29	28
2009	56	36	30	30	27
2010	58	35	32	32	27
2011	63	38	31	30	28
2012	52	33	32	30	25
Average	58.2	35.3	31.1	30.5	27

3.4 Deduction of Complex Propagation Attenuation and Phase Constant

Maxwell's electromagnetic equation was used to obtain the complex propagation coefficients (that is, attenuation and phase constant) in a dust particle medium. The attenuation and phase constant were derived as a function of wave frequency, dielectric constant, depolarization factor and fractional volume of dust particle. However, the attenuation and phase constant can be obtained from equation (2.40) and equation (2.51), depending on the vertical and horizontal polarized wave and the direction of the electric field.

Equations (2.44) and (2.45) were used to obtain the values of attenuation and phase constant of microwave signalpassing through a dusty medium. This puts into consideration the effects of depolarization and the probability distribution of dustin two dimensions (i.e. horizontal and vertical).

3.5 Mathematical Relationship between Visibility and Dust Mass Concentration for Kano Region

Based on the selected values gotten from the extracted data shown in Table 3.1 and Table 3.2, the logarithmic average visibility and mass concentration values were used to obtain a relationship based on the linear graph equation. This was used to obtain the dimensional and dimensionless constants C and γ, respectively, whereby C is the slope and γ is the intercept of the graph. Table 3.3represents the selected values of visibility against dust mass concentration arranged in ascending order.

Table 3.3: Mean Values of Visibility Against Mass Concentration

Visibility (m)	Mass Concentration (Kg/m3)	Log V	Log M
400	0.00000183	2.60206	-5.73754891
420	0.00000177	2.6232493	-5.75202673
620	0.00000125	2.7923917	-5.90308999
1230	0.000000673	3.0899051	-6.17198494
1800	0.000000476	3.2552725	-6.32239305

This was then used to plot a graph as shown in Figure 3.1 so as to obtain the relationship between visibility and mass concentration of dust for Kano region.

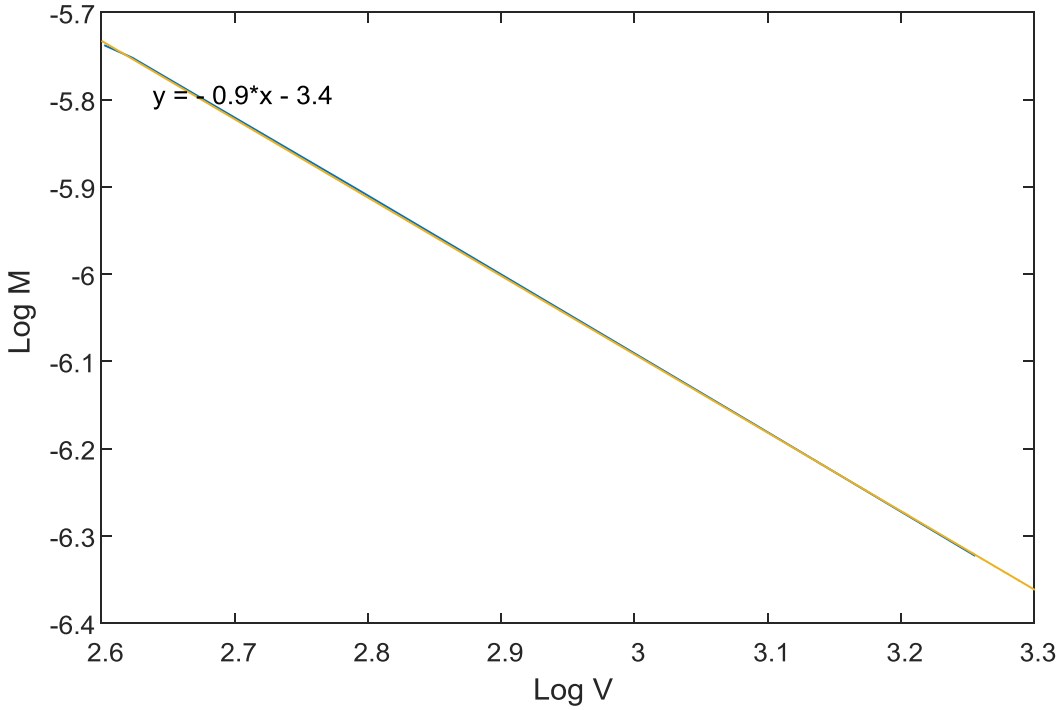

Figure 3.1: Logarithmic Plot of Visibility Against Mass Concentration

From Figure 3.1, it can be seen that the linear graph can be represented by an equation which can be used to obtain both the slope and the intercept of the graph as follows:

$$y = -0.8983x - 3.3969 \tag{3.1}$$

where,

y corresponds to $Log\,M$ and

x corresponds to $Log\,V$

From equation (3.1), the slope was obtained as 0.8983 while the intercept when the value of x equals zero was obtained as follows:

$$\gamma = -0.8983$$

and,

$$Log\,C = -3.3969$$

$$C = 4.01 \times 10^{-4} kg/m^3$$

3.6 Mathematical Relationship for Fractional Volume of Dust Particle

The mass of suspended volume of dust in air which is also termed as fractional volume of dust particle can be obtained based on visibility as shown in subsection 2.4.6.1. This relationship between visibility and suspended volume of dust particle is shown in equation (2.29).

$$V_r = \frac{4.01 \times 10^{-4}}{1.3 \times v^{-0.8983}} \tag{3.2}$$

For each visibility value shown in Table 3.3, the corresponding volume of dust as determined from equation (3.2) is shown in Table 3.4.

Table 3.4: Relative Volume of Dust Particle Against Visibility

Visibility (m)	**Relative Dust Particle Volume, V_r**
400	0.0671
420	0.0701
620	0.0995
1230	0.1840
1800	0.2591

From Table 3.1, the average relative volume of dust during harmattan period in Kano can be obtained as:

$$V = avgV_r = 0.1360 \tag{3.3}$$

3.7 Dielectric Constant for Harmattan Period in Kano Region

The dielectric constant of Kano region for the harmattan period can be obtained using equation (2.30) and equation (2.31), respectively. From Table 2.2, the dielectric constant corresponding to the frequency adopted for this research (that is, 15GHz-38GHz) are 5.1+j1.400 and 4.00+j1.325, respectively. An aggregate dielectric constant,which puts into

consideration the dielectric constant for both frequency bands (that is, the k-band and ka-band) were thenobtained from the individual dielectric constant of each frequency band. Based on the extracted humidity data shown in Table 3.2, a corresponding dielectric constant value for harmattan period in Kano was obtained as follows.

For K-band:

$$\in_{d_1}^{'} = 5.1 + 0.04H - 7.78\times10^{-4}H^2 + 5.56\times10^{-6}H^3 \quad (3.4)$$

$$\in_{d_1}^{''} = 1.4 + 0.02H - 3.71\times10^{-4}H^2 + 2.76\times10^{-6}H^3 \quad (3.5)$$

For the Ka-band:

$$\in_{d_2}^{'} = 4 + 0.04H - 7.78\times10^{-4}H^2 + 5.56\times10^{-6}H^3 \quad (3.6)$$

$$\in_{d_2}^{''} = 1.325 + 0.02H - 3.71\times10^{-4}H^2 + 2.76\times10^{-6}H^3 \quad (3.7)$$

where:

$\in_{d_1}^{'} + j \in_{d_1}^{''}$ represents the complex dielectric constant for K-band

$\in_{d_2}^{'} + j \in_{d_2}^{''}$ represents the complex dielectric constant for Ka-band

The corresponding dielectric values for both frequency bands were then obtained using the sorted humidity data for harmattan period in Kano which is represented in Table 3.2. Since the frequency range considered for this research is between 15 GHz and 38 GHz, a part of this frequency range which is approximately 43.18 percent is covered by the K-band while 56.82 percent is within the Ku-band. Therefore, the aggregate (or average) dielectric constant which was obtained as 0.4318 of k-band and 0.5682 of ka-band can be expressed as:

$$\in_d = 0.4318 \in_{d_1} + 0.5682 \in_{d_2} \quad (3.8)$$

3.8 Particle Size Distribution Function for Kano

The sample data for particle size distribution in Kano was used to obtain the probability distribution function for dust particle. The dust particle size which ranges from 2µm to 291µm was plotted against their respective percentage distributions as illustrated in Figure 3.2.

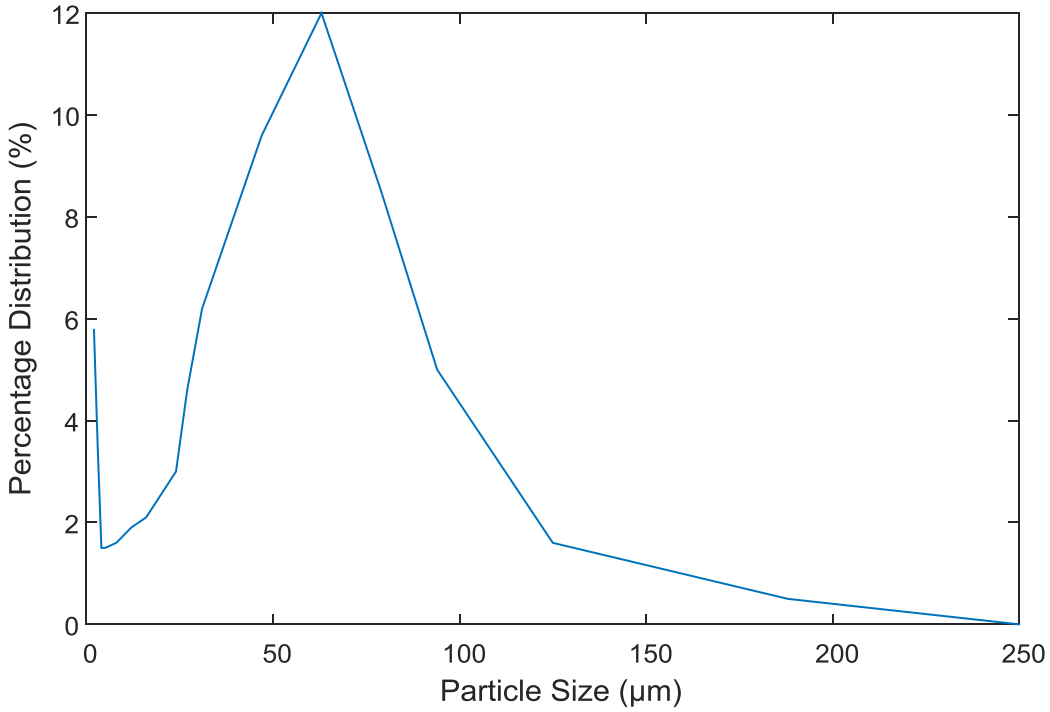

Figure 3.2: Particle Size Distribution in Kano

Figure 3.2 which was plotted from the data shown in Appendix B2 can be represented with a Log-Normal distribution in which for any given distribution, d contained in the total distribution data D, the probability is obtained as follows:

$$P(d < D) = \Phi\left[\frac{\log(d) - \mu}{\sigma^2}\right] \tag{3.9}$$

where;

μ is the mean of the sampled data,

σ is the variance, and

Φ is the standard normal distribution function.

The mean of the distribution sampled data was obtained as 4.21 while the variance is 13.67. Therefore,

$$P(d) = \Phi\left[\frac{\log(d) - 4.21}{186.89}\right] \tag{3.10}$$

Equation (3.10) was used to obtain the probabilities of the dust distribution in the three degrees of freedom as explained in dust particle geometry in section 2.4. Thus the respective values of *'d'* are 0.71 and 0.53 were used to obtain P_1 and P_2 as follows:

$$P_1 = P(0.71) = 0.492 \tag{3.11}$$

$$P_2 = P(0.53) = 0.492 \tag{3.12}$$

3.9 Computation of Cross Polarization Discrimination

In order to obtain the Cross Polarization Discrimination (XPD) for Kano, equation (2.25) was used based on theknown values of horizontal attenuation, vertical attenuation, and depolarization factor.

The horizontal and vertical plane attenuations α_x and α_y are obtained from the values of depolarization factor, dielectric constant, visibility and probability distribution function. Equations (2.50) and (2.51) are thus re-written as follows:

$$\alpha_x = -\frac{\pi}{2\lambda}\sum_n VP_1P_2\,\mathrm{Im}\left(\frac{1}{A_1 + \frac{1}{\in -1}} + \frac{1}{A_2 + \frac{1}{\in -1}}\right) \tag{3.13}$$

$$\alpha_y = -\frac{\pi}{\lambda}\sum_n VP_1P_2\ \mathrm{Im}\left(\frac{1}{A_3+\frac{1}{\in -1}}\right) \tag{3.14}$$

From the vertical and horizontal attenuation expressed by equations (3.13) and (3.14), respectively, the depolarization angle can be obtained as:

$$\delta = \theta - \tan^{-1}\left[\tan\theta\log_{10}^{-1}\left[\frac{-\left(-\frac{\pi f}{2c}\sum VP_1P_2\ \mathrm{Im}\left(\frac{1}{A_1+\frac{1}{\in -1}}+\frac{1}{A_2+\frac{1}{\in -1}}\right)+\frac{\pi f}{c}\sum VP_1P_2\ \mathrm{Im}\left(\frac{1}{A_3+\frac{1}{\in -1}}\right)\right)L}{20}\right]\right]$$

(3.15)

Finally, from equation (2.26), XPD was established as a function of signal frequency, dielectric constant, particle size distribution, and visibility. The corresponding values of XPD for each values of visibility were then obtained.

$$XPD = 20\log\left\{\tan\left[\theta - \tan^{-1}\left[\tan\theta\log_{10}^{-1}\left[\frac{-\left(-\frac{\pi f}{2c}\sum VP_1P_2\ \mathrm{Im}\left(\frac{1}{A_1+\frac{1}{\in -1}}+\frac{1}{A_2+\frac{1}{\in -1}}\right)+\frac{\pi f}{c}\sum VP_1P_2\ \mathrm{Im}\left(\frac{1}{A_3+\frac{1}{\in -1}}\right)\right)L}{20}\right]\right]\right]\right\}$$

(3.16)

Similarly, the loss due to depolarization was obtained using equation (2.54)

3.10 Fade Margin Considering Loss Due to Depolarization

The fade margin factored into the link budget of a typical travelling wave is presented in equation (2.55). However, this research takes care of loss due to depolarization, whereby losses in equation (2.56) are defined as:

$$Losses = FSPL + L_d \tag{3.17}$$

where:

$FSPL$ is the Free-Space Path Loss as given in equation (2.58), and

L_d is the loss due to depolarization.

Substituting equation (3.17) into equation (2.59), and by considering loss due to depolarization, the Fade Margin (FM) wasobtained as:

$$FM = Tx\,Power + Tx\,Gain + Rx\,Gain - FSPL - L_d - receive\,Sensitivity \tag{3.18}$$

Equation (3.18) is re-written as:

$$FM = Tx_P + Tx_G + Rx_G - FSPL - L_d - Rx_S \tag{3.19}$$

Where,

Tx_P *and* Tx_G represent the Transmitter Power and Transmitter Gain respectively,

Rx_G *and* Rx_S represent Receiver Gain and Receive Sensitivity respectively,

By inputting the Free Space Path Loss from equation (2.58) into equation (3.19), FM is expressed as:

$$FM = Tx_P + Tx_G + Rx_G - 20\log_{10}(df) - L_d - Rx_S - 32.45 \tag{3.20}$$

Thus, equation (3.20) wasused to design a link budget template which provides a fade margin for losses due to dust depolarization in Kano.

CHAPTER FOUR

RESULTS AND DISCUSSION

4.1 Introduction

In this Chapter, results obtained are presented and discussed. A mathematical relationship describing cross polarization discrimination as a function of particle size density, visibility, propagation frequency, permittivity, and moisture content of Kano region was first established. The corresponding values of XPD were obtained and a budget template was designed based on fade margin due to XPD degradation.

4.2 Parameter Selection

Certain parameters value and assumptions were obtained from literature and were adopted for simulation purposes. These parameters include:

i. Depolarization factors in the three axes, A1, A2, and A3 are 0.243, 0.324 and 0.432 respectively(Sun *et al.*, 2013).
ii. Elevation angle Ɵ, equals 30^{o}(Elfatih *et al.*, 2013).
iii. Slant path/Path length, L is 1km(Elfatih *et al.*, 2013).
iv. Distance between transmitter and receiver, d is 5km(Tranzeo, 2010).
v. Antenna transmission power is +23dBm(Tranzeo, 2010).
vi. Antenna gain is 24dBi(Tranzeo, 2010).

4.3 Dielectric Constants

The dielectric constant for harmattan period in Kano were obtained from equations (3.4) through equation (3.7). Tables 4.1 and 4.2 representthe corresponding dielectric values for K-band and Ka-band, respectively

Table 4.1: Harmattan Period Dielectric Values for K-Band

Humidity	**Dielectric Constant**	
	E'	**E"**
27	5.7223	1.7239
30.5	5.754	1.7432
31.1	5.7588	1.7462
35.3	5.7871	1.7651
58.2	5.8888	1.8514
Average	5.7822	1.76596

Table 4.1 shows the constant dielectrics for the harmattan period in Kano considered for this research within K-band range. From Table 4.1, it was deduced that the average dielectric constant is:

$$\in_{d_1} = 5.7822 + j1.766 \tag{4.1}$$

Table 4.2: Harmattan Period Dielectric Values for Ka-Band

Humidity	**Dielectric Constant**	
	E'	**E"**
27	4.6223	1.6489
30.5	4.654	1.6682
31.1	4.6588	1.6712
35.3	4.6871	1.6901
58.2	4.7888	1.7764
Average	4.6822	1.6910

Similarly, from Table 4.2, the constant dielectrics for the harmattan period in Kano considered for this research within Ka-band range are presented. From Table 4.2, it was also deduced that the average dielectric constant is:

$$\in_{d_2} = 4.6822 + j1.691 \tag{4.2}$$

Therefore, the total dielectric constant as obtained from equation (3.8) is:

$$\in_{d} = 5.1572 + j1.7234 \tag{4.3}$$

4.4 Result of Attenuation for Harmattan Period in Kano

The values of horizontal attenuation were obtained with respect to visibility using equation (3.13). Each value of the attenuation obtained was the plotted against visibility at frequencies 15GHz, 18GHz, 23GHz, 26GHz, 35GHz and 38GHz respectively as depicted in Figure 4.1. The range of frequencies were selected so as to accommodate the frequency range of this research (that is, between 15GHz and 38GHz) while also considering the commercial microwave transmission frequency in Nigeria which is within the frequency range of this research.

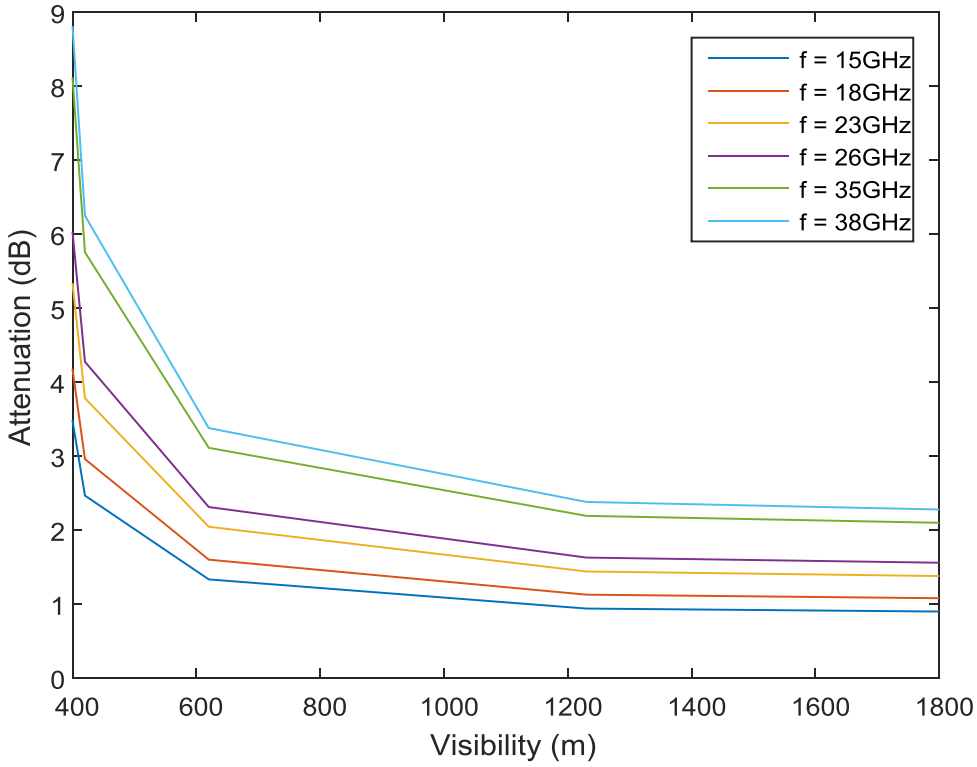

Figure 4.1: Result of Attenuation Against Visibility

From Figure 4.1, it is observed that as the visibility increases, the attenuation reduces irrespective of the frequency of transmission, this is an indication that an increase in dust particle in air can cause an increase in signal attenuation. However, the value of attenuation increases fairly constant value at visibility above 1230m for all frequencies, which indicates that the transmission of the signal is fairly stable beyond this visibility value.

4.5 Result of Cross Polarization Discrimination for Harmattan Period in Kano

The mathematical model expressed by equation (3.16) for obtaining the XPD for harmattan period in Kano was used to obtain the corresponding XPD values with respect to particle size density, visibility, propagation frequency, permittivity, and moisture content. The XPD values obtained based on visibility were plotted against frequency values of 15GHz, 18GHz, 23GHz, 26GHz, 35GHz and 38GHz, respectively as shown in Figure 4.2.

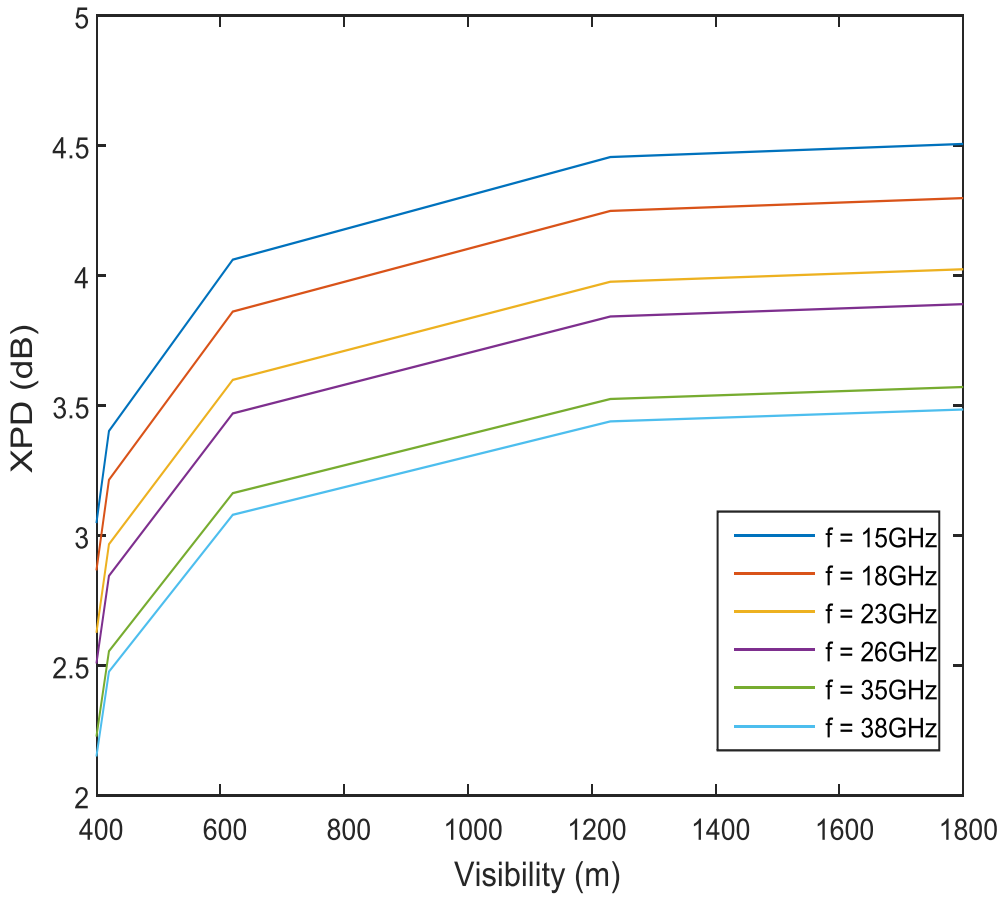

Figure 4.2: Result of XPD Against Visibility

From Figure 4.2, it can be observed that as the visibility increases, the cross polarization discrimination also increases for all frequency of transmission. Therefore, it can be inferred that an increase in dust particle in air causes a corresponding increase in the cross polarization discrimination. At visibility of 1230m and above, the value of XPD is increase fairly constant, thus indicating that signal transmission for all frequencies at 1230m is no longer significantly dependent on visibility.

4.6 Link Budget Design

The parameters of the radiorepresented in Table 2.4 were used in designing a link budget based on Fade Margin while considering loss due to polarization for Kano. Equation (3.20) was used to calculate the fade Margin so as to obtain the reliability of the link using Table 2.3 as a guide. The average relative volume, V which was obtained in equation (3.3) was used to

obtain the values of attenuation for each of the selected frequency before the fade margin was calculated. Hence, Table 4.3 illustrates the results of fade margin for each value of frequency considered in this research.

Table 4.3: Fade Margin Results

Frequency (GHz)	**Fade Margin (dB)**	**Time Availability (%)**
15	52.0731	99.999
18	50.5313	99.999
23	41.2168	99.990
26	43.1843	99.990
35	41.6434	99.990
38	41.3091	99.99

From Table 4.3, it can be concluded that each of the frequencies gives very good availability meaning that the linkwill sufficiently provide a data rate of 200Mbps at more than 99.99 percent availability based on Rayleigh's fading model.

CHAPTER FIVE

CONCLUSION AND RECOMMENDATION

5.1 Summary

This Chapter presents a general summary of this research work. A model for the harmattan dust effect on the cross polarization of a microwave access link operating between 15 GHz and 38GHz was presented. This model put into consideration the effect of loss due to depolarization with regards to its effect on signal attenuation and phase shift when calculating the Cross Polarization Discrimination (XPD) of Kano region. The conclusion, recommendations, and suggestions for further work are also presented below.

5.2 Conclusion

This research work has been able to present a model for harmattan dust effect on cross polarization of a microwave link. In achieving this, dust particle data was collected from Nigerian Meteorological Agency (NIMET) which included dust mass concentration, visibility, particle size distribution, and humidity for Kano region. The visibility and dust mass concentration data were used to obtain a mathematical model for fractional volume of dust particle, while the humidity data was used to deduce a mathematical expression for dielectric constants. The dust particle size distribution was then used to obtain the probability distribution function of dust particle for Kano. The Maxwell's equation in a random medium of dust particle was used to model the propagation coefficients (that is, attenuation and phase constant) as a function of wave frequency, dielectric constant of dust particle, depolarization factor, and fractional volume of dust particle.

A mathematical relationship between Cross Polarization Discrimination (XPD) was then established based on dielectric constant of dust, particle size distribution function, and visibility in Kano before the value of attenuation and XPD were calculated for the frequency range of 15GHz, 18GHz, 23GHz, 26GHz, 35GHz and 38GHz, respectively. Finally, a link

budget based on fade margin was deduced to include depolarization loss using the average fractional dust volume and this showed a maximum percentage time availability of 99.99 percent based on Rayleigh's fading model. This has shown that the model developed for harmattan dust in Kano can be adopted for microwave access radio link operating between 15GHz and 38GHz.

5.3 Significant Contributions

The significant contributions achieved by this research work are as follows:

1. Development of a mathematical model based on visibility and dust mass concentration which was used to obtain the relative volume of dust of 0.0671 to 0.2591 for visibility ranges of 400m to 1800 metres respectively.
2. Development of a mathematical model for XPD based on meteorological data of harmattan period in Kano with specific ranges for the different frequency bands used in this research.
3. Development and deduction of a loss margin due to XPD degradation for link budget analysis with percentage time availability not lower than 99.99 percent.

5.4 Limitations

The limitation of this research work is as follows:

1. Due to challenges of the terrain and the approvals needed from the regulatory body NCC and the security of an Operator's network a prototype was not built to test validity of research

5.3 Recommendations

The following is suggested as recommendation for further work that may be considered as extension of this research:

1. A different mathematical model can be done based on Mie's Theory to see the effect of dust on cross polarization of a microwave access radio link

Reference

Ali, A. A., & Alhaider, M. A. (1992). Millimeter wave propagation in arid land-a field study in Riyadh. *IEEE transactions on antennas and propagation, 40*(5), 492-499.

Bashir, S. O., Musa, A., Hassan, A.-A., & Khalifa, O. O. (2013). Electromagnetic scattering computation methods for very small spheroidal dust particles: Theory and applications. *Middle-East Journal of Scientific Research (Mathematical Applications in Engineering), 13*(13), 38-42.

Bilal, A., Riaz, M., Shafiq, N., Ahmed, M., Sheikh, S., & Rasheed, S. (2015). Non-compliance to anti-hypertensive medication and its associated factors among hypertensives. *JAMC. Journal of Ayub Medical College, Abbottabad, Pakistan, 27*(1), 158-163.

David, A. K., & Moses, O. A. (2011). In situ measurement of soil dielectric permittivity of various soil types across the climatic zones of Nigeria. *International Journal of Physical Sciences, 6*(31), 7139-7148.

Dong, Q., Li, Y., Xu, J., & Wang, M. (2011). Microwave Attenuation and Phase Shift in Sand and Dust Storms.

Eclipse. (2015). ETSI Datasheet: Powers Wireless Backhaul Network *Retrieved March 16, 2016 from*. www.atet.it/...eng/.../Aviat%20Eclipse%20Platform%20Data%20Sheet%20ETSI.pdf.

Elfatih, A., Elsheikh, A., Islam, M., Chebil, J., Bashir, S. O., & Ismail, A. F. (2013). *Preliminary analysis of dust effects on microwave propagation measured in Sudan.* Paper presented at the IOP Conference Series: Materials Science and Engineering, Kuala-Lumpur.

Elshaikh, Z. E. O., Islam, M. R., Khalifa, O. O., & Abd-El-Raouf, H. E. (2009). Mathematical model for the prediction of microwave signal attenuation due to duststorm. *Progress In Electromagnetics Research M, 6*, 139-153.

Elsheikh, E. A., Islam, M. R., Alam, A. Z., Ismail, A. F., Al-Khateeb, K., & Elabdin, Z. (2010). *The effect of particle size distributions on dust storm attenuation prediction for microwave propagation.* Paper presented at the Computer and Communication Engineering (ICCCE), 2010 International Conference on.

Freeman, R. L. (2005). *Fundamentals of telecommunications* (Vol. 92): John Wiley & Sons.

Ghobrial, S., & Sharief, S. (1987). Microwave attenuation and cross polarization in dust storms. *IEEE transactions on antennas and propagation, 35*(4), 418-425.

Harb, K., Butt, O., Abdul-Jauwad, S., & Al-Yami, A. M. (2013). Systems adaptation for satellite signal under dust, sand and gaseous attenuations. *Journal of Wireless Networking and Communications, 3*(3), 39-49.

Hong, G., Yang, P., Weng, F., & Liu, Q. (2008). Microwave scattering properties of sand particles: Application to the simulation of microwave radiances over sandstorms. *Journal of Quantitative Spectroscopy and Radiative Transfer, 109*(4), 684-702.

Islam, M., Elabdin, Z., Elshaikh, O., Khalifa, O. O., Alam, A., Khan, S., & Naji, A. W. (2010). Prediction of signal attenuation due to duststorms using Mie scattering. *IIUM Engineering Journal, 11*(1), 71-87.

Jakes, W. C., & Cox, D. C. (1994). *Microwave mobile communications*: Wiley-IEEE Press.

Kesavan, U., Tharek, A., & Islam, M. R. (2012). *Comparison of Microwave Path Lengths between Temperate and Tropical Region Based on Effects of Rain.* Paper presented at the Progress in Electromagnetic Research Symposium (PIERS), Proceedings Moscow, Russia.

Kok, J. F., Parteli, E. J., Michaels, T. I., & Karam, D. B. (2012). The physics of wind-blown sand and dust. *Reports on Progress in Physics, 75*(10), 106901.

Liu, C., Zhang, L., Peng, J., Srinivasakannan, C., Liu, B., Xia, H., . . . Xu, L. (2013). Temperature and moisture dependence of the dielectric properties of silica sand. *Journal of Microwave Power and Electromagnetic Energy, 47*(3), 199-209.

Manning, R. (2009). *Using indicators to encourgae development: Lessons from the millennium development goals* (Vol. 2009: 01): DIIS Reports/Danish Institute for International Studies.

McTainsh, G. (1984). The nature and origin of the aeolian mantles of central northern Nigeria. *Geoderma, 33*(1), 13-37.

Musa, A., & Bashir, S. (2013). Prediction of cross polarization discrimination at millimeter wave band due to dust storms. *ARPN Journal of Engineering and Applied Sciences, 8*(7), 465-472.

Musa, A., Bashir, S. O., & Abdalla, A. H. (2014a). Review and Assessment of Electromagnetic Wave Propagation in Sand and Dust Storms at Microwave and Millimeter Wave Bands---Part I. *Progress In Electromagnetics Research M, 40*, 91-100.

Musa, A., Bashir, S. O., & Abdalla, A. H. (2014b). Review and Assessment of Electromagnetic Wave Propagation in Sand and Dust Storms at Microwave and Millimeter Wave Bands---Part II. *Progress In Electromagnetics Research M, 40*, 101-110.

Rai, C. (2012). Depolarization of millimeter wave due to non-spherical dust particles in storms. *Indian Journal of Physics, 86*(8), 709-714.

Reid, R. D., & Sanders, N. R. (2005). *Operations management: an integrated approach*: John Wiley Hoboken, NJ.

Saleh, I., & Abuhdima, E. (2011). Effect of sand and dust storms on microwave propagation signals in Southern Libya. *Journal of Energy and Power Engineering, 5*(12).

Shao, Y. (2008). *Physics and modelling of wind erosion* (Vol. 37): Springer Science & Business Media.

Sharif, S. M. (2015). Dust storms properties related to microwave signal propagation.

Sun, X., Cao, Y., & Che, J. (2013). A Simulation Study on Channel Estimation for Cooperative Communication System in Sand-dust Storm Environment. *Communications and Network, 5*(03), 15-17.

Syvitski, J. P. (2007). Principles, methods and application of particle size analysis (pp. 1247): Cambridge University Press.

Topp, G. C., Davis, J., & Annan, A. P. (1980). Electromagnetic determination of soil water content: Measurements in coaxial transmission lines. *Water resources research, 16*(3), 574-582.

Tranzeo, W. T. I. (2010). Wireless Link Budget Analysis. *Retrieved March 16, 2016 from*

http://www.tranzeo.com/allowed/Tranzeo_Link_Budget_Whitepaper.pdf

Vyas, M., Tomar, P., Rankawat, S., & Godara, D. (2014). Effect of sand and dust storms on millimeter wave propagation signals in western Rajasthan region at 35 GHz. *International Journal of Scientific Research And Education, 2*(11).

Wikner, D. (2008). Millimeter-wave propagation measurement through a dust tunnel: DTIC Document. *Army Research Lab Adelphi MD Sensors and Electron Devices Directorate*

Appendix A1

Monthly Visibility Data for Kano Region (NIMET)

m)	March	April	May	June	July	August	September	Oc
	4810	4770	3610	8920	5610	6300	1780	
	5010	5400	10460	17900	5380	8670	4650	
	3170	7160	14450	10560	8320	5030	7600	
	4920	2990	19360	2860	11570	10870	2430	
	3810	8180	4920	8910	6680	9380	5760	
	20300	9100	10350	8670	9100	4830	3470	
	100	4170	5380	10800	9210	4790	2700	
	8240	3880	2120	11010	4920	3450	2560	
	3080	6840	1150	5070	2410	7280	3950	
	2260	5010	7100	10000	0	0	0	
	5570	5750	7890	9470	6320	6060	3490	

Appendix A2

Monthly Percentage Humidity Data for Kano Region (NIMET)

6)	March	April	May	June	July	August	September	Oc
	26	35	53	59	77	83	79	
	26	37	54	65	74	81	74	
	26	37	49	65	79	81	73	
	25	36	51	57	74	82	73	
	26	38	51	57	77	85	77	
	25	35	53	62	78	82	75	
	26	36	53	69	80	85	74	
	25	36	53	69	81	81	78	
	25	38	55	70	78	80	78	
	27	35	48	55	75	86	73	
	25.7	36.3	52	62.8	77.3	82.6	75.4	

Appendix B1

Dust Mass Concentration per Visibility Data for Kano Region (NIMET)

Dust Concentration per Visibility	
Visibility (m)	**Mass Concentration (Kg/m3)**
400	0.00000183
420	0.00000177
620	0.00000125
1230	0.000000673
1800	0.000000476
3490	0.000000263
5570	0.000000172
5750	0.000000167
6060	0.00000016
6320	0.000000154
7890	0.000000126
9470	0.000000107

Appendix B2

Percentage Particle Size Distribution Data for Kano Region (NIMET)

Percentage Particle Size Distribution		
Particle Size (um)	**% Distribution**	
2	5.8	5.8
3	3.5	3.5
4	1.5	1.5
5	1.5	1.5
8	1.6	1.6
12	1.9	1.9
16	2.1	2.1
24	3	3
27	4.6	4.6
31	6.2	6.2
47	9.6	9.6
55	10.8	10.8
63	12	12
79	8.5	8.5
94	5	5
125	1.6	1.6
188	0.5	0.5
219	0.25	0.25
250	0	0

Appendix C1

Standard Normal Distribution Table(Reid & Sanders, 2005)

Z	Φ (z)	φ (z)	*z*	Φ (z)	φ (z)	*z*	Φ (z)	φ (z)	*z*	Φ (z)	φ (z)
0	0.5	0.3989	1	0.8413	0.242	2	0.9772	0.054	3	0.9987	0.0044
0.01	0.504	0.3989	1.01	0.8438	0.2396	2.01	0.9778	0.0529	3.01	0.9987	0.0043
0.02	0.508	0.3989	1.02	0.8461	0.2371	2.02	0.9783	0.0519	3.02	0.9987	0.0042
0.03	0.512	0.3988	1.03	0.8485	0.2347	2.03	0.9788	0.0508	3.03	0.9988	0.004
0.04	0.516	0.3986	1.04	0.8508	0.2323	2.04	0.9793	0.0498	3.04	0.9988	0.0039
0.05	0.5199	0.3984	1.05	0.8531	0.2299	2.05	0.9798	0.0488	3.05	0.9989	0.0038
0.06	0.5239	0.3982	1.06	0.8554	0.2275	2.06	0.9803	0.0478	3.06	0.9989	0.0037
0.07	0.5279	0.398	1.07	0.8577	0.2251	2.07	0.9808	0.0468	3.07	0.9989	0.0036
0.08	0.5319	0.3977	1.08	0.8599	0.2227	2.08	0.9812	0.0459	3.08	0.999	0.0035
0.09	0.5359	0.3973	1.09	0.8621	0.2203	2.09	0.9817	0.0449	3.09	0.999	0.0034
0.1	0.5398	0.397	1.1	0.8643	0.2179	2.1	0.9821	0.044	3.1	0.999	0.0033
0.11	0.5438	0.3965	1.11	0.8665	0.2155	2.11	0.9826	0.0431	3.11	0.9991	0.0032
0.12	0.5478	0.3961	1.12	0.8686	0.2131	2.12	0.983	0.0422	3.12	0.9991	0.0031
0.13	0.5517	0.3956	1.13	0.8708	0.2107	2.13	0.9834	0.0413	3.13	0.9991	0.003
0.14	0.5557	0.3951	1.14	0.8729	0.2083	2.14	0.9838	0.0404	3.14	0.9992	0.0029
0.15	0.5596	0.3945	1.15	0.8749	0.2059	2.15	0.9842	0.0396	3.15	0.9992	0.0028
0.16	0.5636	0.3939	1.16	0.877	0.2036	2.16	0.9846	0.0387	3.16	0.9992	0.0027
0.17	0.5675	0.3932	1.17	0.879	0.2012	2.17	0.985	0.0379	3.17	0.9992	0.0026
0.18	0.5714	0.3925	1.18	0.881	0.1989	2.18	0.9854	0.0371	3.18	0.9993	0.0025
0.19	0.5753	0.3918	1.19	0.883	0.1965	2.19	0.9857	0.0363	3.19	0.9993	0.0025
0.2	0.5793	0.391	1.2	0.8849	0.1942	2.2	0.9861	0.0355	3.2	0.9993	0.0024
0.21	0.5832	0.3902	1.21	0.8869	0.1919	2.21	0.9864	0.0347	3.21	0.9993	0.0023
0.22	0.5871	0.3894	1.22	0.8888	0.1895	2.22	0.9868	0.0339	3.22	0.9994	0.0022
0.23	0.591	0.3885	1.23	0.8907	0.1872	2.23	0.9871	0.0332	3.23	0.9994	0.0022
0.24	0.5948	0.3876	1.24	0.8925	0.1849	2.24	0.9875	0.0325	3.24	0.9994	0.0021
0.25	0.5987	0.3867	1.25	0.8944	0.1826	2.25	0.9878	0.0317	3.25	0.9994	0.002
0.26	0.6026	0.3857	1.26	0.8962	0.1804	2.26	0.9881	0.031	3.26	0.9994	0.002
0.27	0.6064	0.3847	1.27	0.898	0.1781	2.27	0.9884	0.0303	3.27	0.9995	0.0019
0.28	0.6103	0.3836	1.28	0.8997	0.1758	2.28	0.9887	0.0297	3.28	0.9995	0.0018
0.29	0.6141	0.3825	1.29	0.9015	0.1736	2.29	0.989	0.029	3.29	0.9995	0.0018
0.3	0.6179	0.3814	1.3	0.9032	0.1714	2.3	0.9893	0.0283	3.3	0.9995	0.0017
0.31	0.6217	0.3802	1.31	0.9049	0.1691	2.31	0.9896	0.0277	3.31	0.9995	0.0017
0.32	0.6255	0.379	1.32	0.9066	0.1669	2.32	0.9898	0.027	3.32	0.9995	0.0016
0.33	0.6293	0.3778	1.33	0.9082	0.1647	2.33	0.9901	0.0264	3.33	0.9996	0.0016
0.34	0.6331	0.3765	1.34	0.9099	0.1626	2.34	0.9904	0.0258	3.34	0.9996	0.0015
0.35	0.6368	0.3752	1.35	0.9115	0.1604	2.35	0.9906	0.0252	3.35	0.9996	0.0015
0.36	0.6406	0.3739	1.36	0.9131	0.1582	2.36	0.9909	0.0246	3.36	0.9996	0.0014
0.37	0.6443	0.3725	1.37	0.9147	0.1561	2.37	0.9911	0.0241	3.37	0.9996	0.0014
0.38	0.648	0.3712	1.38	0.9162	0.1539	2.38	0.9913	0.0235	3.38	0.9996	0.0013
0.39	0.6517	0.3697	1.39	0.9177	0.1518	2.39	0.9916	0.0229	3.39	0.9997	0.0013

Standard Normal Distribution Table

0.4	0.6554	0.3683	1.4	0.9192	0.1497	2.4	0.9918	0.0224	3.4	0.9997	0.0012
0.41	0.6591	0.3668	1.41	0.9207	0.1476	2.41	0.992	0.0219	3.41	0.9997	0.0012
0.42	0.6628	0.3653	1.42	0.9222	0.1456	2.42	0.9922	0.0213	3.42	0.9997	0.0012
0.43	0.6664	0.3637	1.43	0.9236	0.1435	2.43	0.9925	0.0208	3.43	0.9997	0.0011
0.44	0.67	0.3621	1.44	0.9251	0.1415	2.44	0.9927	0.0203	3.44	0.9997	0.0011
0.45	0.6736	0.3605	1.45	0.9265	0.1394	2.45	0.9929	0.0198	3.45	0.9997	0.001
0.46	0.6772	0.3589	1.46	0.9279	0.1374	2.46	0.9931	0.0194	3.46	0.9997	0.001
0.47	0.6808	0.3572	1.47	0.9292	0.1354	2.47	0.9932	0.0189	3.47	0.9998	0.001
0.48	0.6844	0.3555	1.48	0.9306	0.1334	2.48	0.9934	0.0184	3.48	0.9998	0.0009
0.49	0.6879	0.3538	1.49	0.9319	0.1315	2.49	0.9936	0.018	3.49	0.9998	0.0009
0.5	0.6915	0.3521	1.5	0.9332	0.1295	2.5	0.9938	0.0175	3.5	0.9998	0.0009
0.51	0.695	0.3503	1.51	0.9345	0.1276	2.51	0.994	0.0171	3.51	0.9998	0.0008
0.52	0.6985	0.3485	1.52	0.9357	0.1257	2.52	0.9941	0.0167	3.52	0.9998	0.0008
0.53	0.7019	0.3467	1.53	0.937	0.1238	2.53	0.9943	0.0163	3.53	0.9998	0.0008
0.54	0.7054	0.3448	1.54	0.9382	0.1219	2.54	0.9945	0.0158	3.54	0.9998	0.0008
0.55	0.7088	0.3429	1.55	0.9394	0.12	2.55	0.9946	0.0154	3.55	0.9998	0.0007
0.56	0.7123	0.341	1.56	0.9406	0.1182	2.56	0.9948	0.0151	3.56	0.9998	0.0007
0.57	0.7157	0.3391	1.57	0.9418	0.1163	2.57	0.9949	0.0147	3.57	0.9998	0.0007
0.58	0.719	0.3372	1.58	0.9429	0.1145	2.58	0.9951	0.0143	3.58	0.9998	0.0007
0.59	0.7224	0.3352	1.59	0.9441	0.1127	2.59	0.9952	0.0139	3.59	0.9998	0.0006
0.6	0.7257	0.3332	1.6	0.9452	0.1109	2.6	0.9953	0.0136	3.6	0.9998	0.0006
0.61	0.7291	0.3312	1.61	0.9463	0.1092	2.61	0.9955	0.0132	3.61	0.9998	0.0006
0.62	0.7324	0.3292	1.62	0.9474	0.1074	2.62	0.9956	0.0129	3.62	0.9999	0.0006
0.63	0.7357	0.3271	1.63	0.9484	0.1057	2.63	0.9957	0.0126	3.63	0.9999	0.0005
0.64	0.7389	0.3251	1.64	0.9495	0.104	2.64	0.9959	0.0122	3.64	0.9999	0.0005
0.65	0.7422	0.323	1.65	0.9505	0.1023	2.65	0.996	0.0119	3.65	0.9999	0.0005
0.66	0.7454	0.3209	1.66	0.9515	0.1006	2.66	0.9961	0.0116	3.66	0.9999	0.0005
0.67	0.7486	0.3187	1.67	0.9525	0.0989	2.67	0.9962	0.0113	3.67	0.9999	0.0005
0.68	0.7517	0.3166	1.68	0.9535	0.0973	2.68	0.9963	0.011	3.68	0.9999	0.0005
0.69	0.7549	0.3144	1.69	0.9545	0.0957	2.69	0.9964	0.0107	3.69	0.9999	0.0004
0.7	0.758	0.3123	1.7	0.9554	0.094	2.7	0.9965	0.0104	3.7	0.9999	0.0004
0.71	0.7611	0.3101	1.71	0.9564	0.0925	2.71	0.9966	0.0101	3.71	0.9999	0.0004
0.72	0.7642	0.3079	1.72	0.9573	0.0909	2.72	0.9967	0.0099	3.72	0.9999	0.0004
0.73	0.7673	0.3056	1.73	0.9582	0.0893	2.73	0.9968	0.0096	3.73	0.9999	0.0004
0.74	0.7704	0.3034	1.74	0.9591	0.0878	2.74	0.9969	0.0093	3.74	0.9999	0.0004
0.75	0.7734	0.3011	1.75	0.9599	0.0863	2.75	0.997	0.0091	3.75	0.9999	0.0004
0.76	0.7764	0.2989	1.76	0.9608	0.0848	2.76	0.9971	0.0088	3.76	0.9999	0.0003
0.77	0.7794	0.2966	1.77	0.9616	0.0833	2.77	0.9972	0.0086	3.77	0.9999	0.0003
0.78	0.7823	0.2943	1.78	0.9625	0.0818	2.78	0.9973	0.0084	3.78	0.9999	0.0003
0.79	0.7852	0.292	1.79	0.9633	0.0804	2.79	0.9974	0.0081	3.79	0.9999	0.0003
0.8	0.7881	0.2897	1.8	0.9641	0.079	2.8	0.9974	0.0079	3.8	0.9999	0.0003
0.81	0.791	0.2874	1.81	0.9649	0.0775	2.81	0.9975	0.0077	3.81	0.9999	0.0003
0.82	0.7939	0.285	1.82	0.9656	0.0761	2.82	0.9976	0.0075	3.82	0.9999	0.0003

Standard Normal Distribution Table

0.83	0.7967	0.2827	1.83	0.9664	0.0748	2.83	0.9977	0.0073	3.83	0.9999	0.0003
0.84	0.7995	0.2803	1.84	0.9671	0.0734	2.84	0.9977	0.0071	3.84	0.9999	0.0003
0.85	0.8023	0.278	1.85	0.9678	0.0721	2.85	0.9978	0.0069	3.85	0.9999	0.0002
0.86	0.8051	0.2756	1.86	0.9686	0.0707	2.86	0.9979	0.0067	3.86	0.9999	0.0002
0.87	0.8078	0.2732	1.87	0.9693	0.0694	2.87	0.9979	0.0065	3.87	0.9999	0.0002
0.88	0.8106	0.2709	1.88	0.9699	0.0681	2.88	0.998	0.0063	3.88	0.9999	0.0002
0.89	0.8133	0.2685	1.89	0.9706	0.0669	2.89	0.9981	0.0061	3.89	0.9999	0.0002
0.9	0.8159	0.2661	1.9	0.9713	0.0656	2.9	0.9981	0.006	3.9	1	0.0002
0.91	0.8186	0.2637	1.91	0.9719	0.0644	2.91	0.9982	0.0058	3.91	1	0.0002
0.92	0.8212	0.2613	1.92	0.9726	0.0632	2.92	0.9982	0.0056	3.92	1	0.0002
0.93	0.8238	0.2589	1.93	0.9732	0.062	2.93	0.9983	0.0055	3.93	1	0.0002
0.94	0.8264	0.2565	1.94	0.9738	0.0608	2.94	0.9984	0.0053	3.94	1	0.0002
0.95	0.8289	0.2541	1.95	0.9744	0.0596	2.95	0.9984	0.0051	3.95	1	0.0002
0.96	0.8315	0.2516	1.96	0.975	0.0584	2.96	0.9985	0.005	3.96	1	0.0002
0.97	0.834	0.2492	1.97	0.9756	0.0573	2.97	0.9985	0.0048	3.97	1	0.0002
0.98	0.8365	0.2468	1.98	0.9761	0.0562	2.98	0.9986	0.0047	3.98	1	0.0001
0.99	0.8389	0.2444	1.99	0.9767	0.0551	2.99	0.9986	0.0046	3.99	1	0.0001

Appendix D

MATLAB Codes

```
% horizontal and vertical attenuation
clc
V=[0.0671 0.0701 0.0995 0.1840 0.2591];  %relative volume
vi = [400 420 620 1230 1800];   %visibility
vii = [1800 1230 620 420 400];
f1=[15e9:1e9:38e9];%frequency
f=[15e9 18e9 23e9 26e9 35e9 38e9];%frequency
A1=0.243;
A2=0.324;
A3=0.432;
c=299792458;
L=1000;
P1=0.492;
P2=0.492;
theta=30;
sgm=5.1572-1.7234i;  %Sigma i.e dielectric
p=(((((-pi*f(:)*V*P1*P2)/(2*c))*imag((1/(A1+(1/(sgm-1))))+(1/(A2+(1/(sgm-
1)))))+(((pi*f(:)*V*P1*P2)/c)*imag(1/(A3+(1/(sgm-1)))))*L);
ps1=-log10(p);
ps=tan(theta)*(ps1.^-1);

psi=theta-atan(ps)
XPD=-20*log10(tan(psi))
plot(vii,XPD)
% horizontal and vertical attenuation
clc
V=0.136;  %relative volume
vi = [400 420 620 1230 1800];   %visibility
vii = [1800 1230 620 420 400];
f=[15e9 18e9 23e9 26e9 38e9];%frequency
A1=0.243;
A2=0.324;
A3=0.432;
c=299792458;
P1=0.492;
P2=0.492;
Txp=[16.5 16.5 12.5 15 15 ];
Txg=[88 87.5 82 83.5 83.5 ];
Rxg=[88 87.5 82 83.5 83.5 ];
Rxs=[-71.5 -71 -69.5 -69 -68.5];
k=[32.5 32.5 32.5 32.5 32.5 ];
theta=30;
d= 3000;
L=1000;
sgm=5.1572-1.7234i;  %Sigma i.e dielectric
```

```
Alphax=((-pi*f(:)*V*P1*P2)/(2*c))*imag((1/(A1+(1/(sgm-1))))+(1/(A2+(1/(sgm-1)))));
Alphay=((-pi*f(:)*V*P1*P2)/(2*c))*imag((1/(A1+(1/(sgm-1)))))
df=4*pi*d*f/c;
ldf=20*(log10(df));
%plot(vii,Alphay)
L1=atan(log10((Alphax-Alphay)*(L/20)));
L2=((cos(theta-L1)).^2).\1;
Ld=10*log10(L2)
FM=Txp+Txg+Rxg-Rxs-k-ldf-Ld(5,:)
% horizontal and vertical attenuation
clc
V=[0.0671 0.0701 0.0995 0.1840 0.2591];  %relative volume
vi = [400 420 620 1230 1800];   %visibility
vii = [1800 1230 620 420 400];
f1=[15e9:1e9:38e9];%frequency
f=[15e9 18e9 23e9 26e9 35e9 38e9];%frequency
A1=0.243;
A2=0.324;
A3=0.432;
c=299792458;
P1=0.492;
P2=0.492;
sgm=5.1572-1.7234i;  %Sigma i.e dielectric
Alphax=((-pi*f(:)*V*P1*P2)/(2*c))*imag((1/(A1+(1/(sgm-1))))+(1/(A2+(1/(sgm-1)))))
plot(vii,Alphax)% horizontal and vertical attenuation
clc
V=[0.0085 0.0089 0.0126 0.0233 0.0328];  %relative volume
vi = [400 420 620 1230 1800];   %visibility
vii = [1800 1230 620 420 400];
f1=[15e9:1e9:38e9];%frequency
f=[18e9 25e9 27e9 30e9 35e9];%frequency
A1=0.243;
A2=0.324;
A3=0.432;
c=299792458;
P1=0.492;
P2=0.492;
sgm=5.1572-1.7234i;  %Sigma i.e dielectric
Alphax=((-pi*f(:)*V*P1*P2)/(2*c))*real((1/(A1+(1/(sgm-1))))+(1/(A2+(1/(sgm-1)))))
plot(vii,Alphax)
```

Published with MATLAB® R2015b